Recent progress in synthesis and application of mussel-inspired adhesives

Guo, Qi; Chen, Jingsi; Wang, Jilei; Zeng, Hongbo; Yu, Jing

2019

Guo, Q., Chen, J., Wang, J., Zeng, H., & Yu, J. (2020). Recent progress in synthesis and application of mussel-inspired adhesives. Nanoscale, 12(3), 1307-1324. doi:10.1039/C9NR09780E

https://hdl.handle.net/10356/138103

https://doi.org/10.1039/C9NR09780E

Recent Progress in Synthesis and Application of Mussel-Inspired Adhesives

Qi Guo[1,§], Jingsi Chen[2,§], Jilei Wang[1], Hongbo Zeng[2,*], Jing Yu[1,*]

[1]*School of Materials Science and Engineering, Nanyang Technological University, Singapore*

[2]*Department of Chemical and Materials Engineering, University of Alberta, Edmonton, Alberta T6G 1H9, Canada*

[§] *Q Guo and J Chen contributed equally to this work*

**Email: Hongbo.Zeng@ualberta.ca (H. Zeng), yujing@ntu.edu.sg (J. Yu),*

ABSTRACT

The rapid and robust adhesion of marine mussels to diverse solid surfaces in wet environments is mediated by the secreted mussel adhesive proteins which are abundant in a catecholic amino acid, *L*-3,4-dihydroxyphenylalanine (Dopa). Over the last two decades, enormous efforts have been devoted to the development of synthetic mussel-inspired adhesives with water-resistant adhesion and cohesion properties by modifying polymer systems with Dopa and its analogues. In the present review, an overview of the unique features of various mussel foot proteins is provided in combination with an up-to-date understanding of catechol chemistry, which contributes to the strong interfacial binding via balancing a variety of covalent and noncovalent interactions including oxidative cross-linking, electrostatic interaction, metal-catechol coordination, hydrogen bonding, hydrophobic interactions and π–π/cation-π interactions. The recent developments of novel Dopa-containing adhesives with on-demand mechanical properties and other functionalities are then summarized under four broad categories: viscous coacervated adhesives, soft adhesive hydrogels, smart adhesives, and stiff adhesive polyesters, where their emerging applications in

engineering, biological and biomedical fields are discussed. Limitations of the developed adhesives are identified and future research perspectives in this field are proposed.

I INTRODUCTION

One grand challenge in material engineering is to engineer materials with strong adhesive properties in the moist environment [1, 2] since water has been known as a barrier to robust and durable adhesion. At the molecular level, interfacial water molecules can prevent the forming of adhesive bonds between the adhesives and the target surfaces, leading to weak adhesive binding even failure of the adhesives [3, 4]. Marine mussels have mastered wet adhesion with strong attachment to a diversity of substrates in seawater by a holdfast structure known as the byssus, where a family of adhesive proteins (Fig 1a) [5, 6]containing a post-translationally modified amino acid *L*-3,4-dihydroxyphenylalanine (Dopa). These mussel foot proteins (Mfps), also known as the mussel adhesive proteins, have strong wet adhesion on various surfaces through Dopa-mediated interfacial bonding. Over the years, researchers have paid great efforts to artificially synthesize adhesives, especially polymers containing catecholic functional groups, which mimic the adhesive proteins of mussels for various practical applications requiring underwater adhesion, ranging from tissue sealants to functional coatings. The interaction mechanisms of the mussel-inspired, water-resistant adhesives and coating materials to different surfaces such as mica, SiO_2, poly(methyl methacrylate) (PMMA), polystyrene (PS), TiO_2, gold, metal oxides and organic thin films have attracted numerous interests for potential application in different fields, like biomedicine [7-11]. The insights obtained from the understanding of the interaction mechanisms between individual mussel foot proteins (Mfps) and disparate substrates provide critical guidance for the design of next-generation wet adhesive materials [12-15].

This review covers recent progress on the design of adhesive materials derived from Mfps by focusing on two aspects: the adhesive mechanism of Mfps and the preparation of mussel-inspired

polymers. Comparing to other literature reviews on Mussel-inspired adhesives[16-21], our review focuses more on the molecular mechanisms of mussel adhesion. We firstly describe the unique characteristics of some key proteins identified in the adhesive plaque of mussels and several essential factors influencing their functionalities. We then summarize the recent achievements in developing novel mussel-inspired materials, which involves Dopa-functionalized adhesives including coacervates [1, 15, 22, 23], adhesive hydrogels [20, 24-27], smart adhesives [28-31] and adhesive polyesters [32-35], holding great promise for a wide range of applications, including biomedicine [7-11], bioreactors[36-38], coating materials [1, 23, 31, 39, 40] and drug delivery [41-43].

II MUSSEL ADHESIVE PROTEINS

2.1 Mussel Foot Proteins

The mussel foot possesses an important functionality in term of synthesis, sensing and building. The entire byssus is produced in its ventral groove with one thread each time and the major component of the byssus thread is collagen (>90 wt%) (ref). The byssus takes function as a bundle of threads composed of proteins, and each of the thread links to an adhesive plaque at the distal end (Fig 1a). To overcome the mismatch between mussel body and the marine substrates, mussels employ byssus threads with a gradient stiffness. Such gradient byssus is achieved by the time-regulated secretion, beginning with the interfacial proteins at the distal end, then bulk proteins in the plaque and thread components[21]. A new plaque can be assembled by the mussel in a few minutes after the secretion of proteins [44].

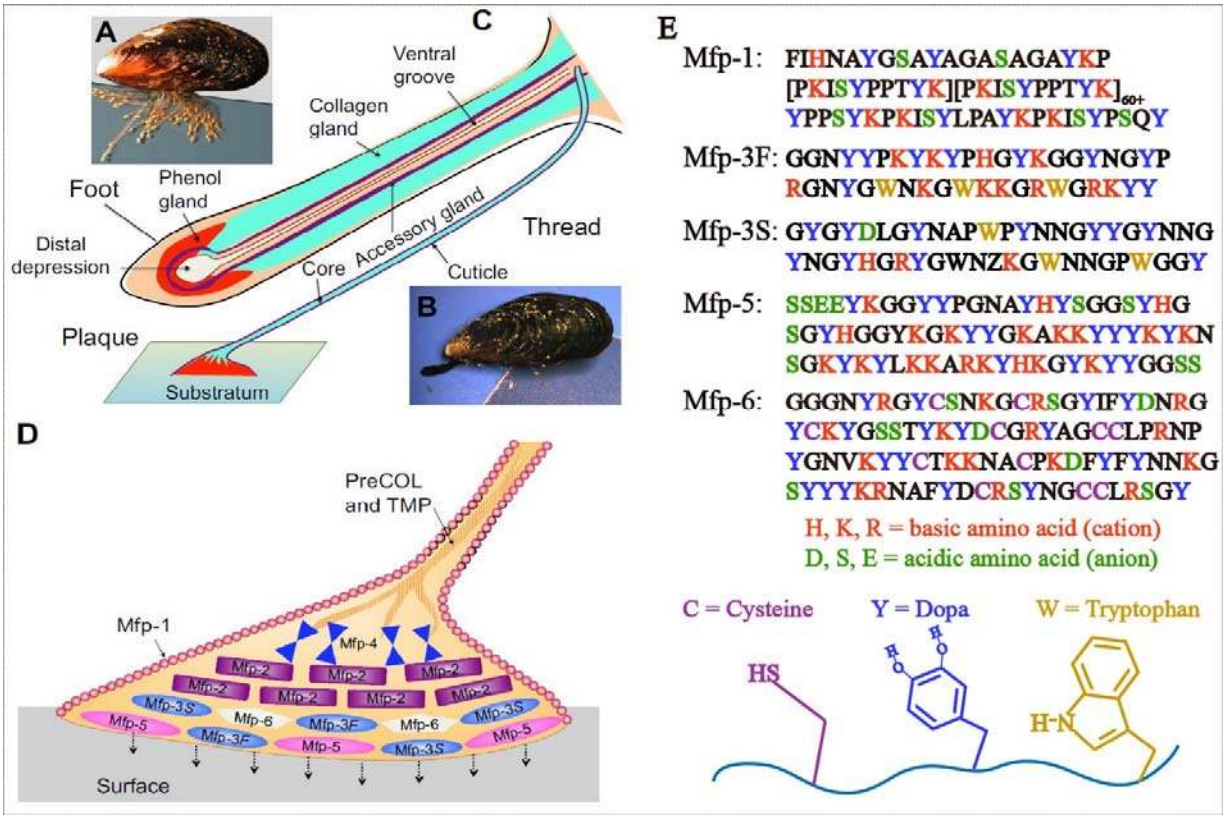

Fig. 1 Mytilus mussels. (a) A view of the mussel byssus from the base of the foot that distally attaches to the substratum. (b) Underside schematic view of a mussel foot indicates the distal depression lifting off from a completed plaque. The most distal part of a plaque attaching to the substrate surface is denoted in the footprint. The specific byssal proteins are synthesized and stockpiled by three gland clusters: accessory glands, phenol, and collagen. (c) Schematic distribution representation of as-studied proteins in the byssal plaque and at the distal end of thread. (d) Primary sequence of selected footprint protein variants of Mfp-1, Mfp-3S, Mfp-3F, Mfp-5, and Mfp-6 containing C (Cys), R (Arg) and K (Lys), G (Gly) and Y (Tyr). Color: blue (Y/Dopa), red (cationic side chains: H, K, R), green (anionic side chains: D, S, E) and purple (thiols). Reproduced with permission [45]. Copyright © 2017, COMPANY OF BIOLOGISTS LTD

Based on the reports [4, 45-66], the byssus consists of 20 different known protein components. Most of the proteins exhibit highly localized distributions, and many of them have not yet been fully characterized. At least twelve proteins within the adhesive plaques have been investigated for *Mytilus* species, and several of them are intensively characterized with mass, isoelectric point (pI), post-translational modifications, structure and locations in the plaque (Table 1) [4, 45-66]. The six

important plaque proteins namely Mfp through 1–6 [4, 45-66]are generated from the major glands of the mussel foot and destined for the plaque (Figure 1b). All of these proteins contain different ratios of Dopa residue, derived from hydroxylation of tyrosine residue within the post-translational modification process. (Fig 1c, d). By injecting KCl to trigger the plaque protein secretion process, time-regulated secretion sequence is decrypted as Mfp-3 variants, Mfp-5 and Mfp-6 secreted within seconds to initial adhesion, then Mfp-2 and Mfp-4 comprising the foamy interior[67, 68]. A similar process has been reported for the *Perna* green mussel[69].

Mfp-1 is a coating protein of the byssal cuticle with high molecular weight (~ 110 kDa) and possesses local polyproline II structures [46-48]. It functions as a protective layer with a combination of both high stiffness and extensibility, and presents in the cuticle of the byssus threads of the adhesive plaques. The most abundant protein (25 wt %) in the plaques is Mfp-2, with a mass of 45 kDa found in *M. edulis*. Located within the plaque, Mfp-2 contains highly repetitive motifs and epidermal growth factor-like local structure connected by irregular sequences [70]. It is reported that the repeated regions of localized structure are only 5 to 6 residues in length (PPII) in Mfp-1, but for Mfp-2 the amount of repeated regions increases to about 40 residues in length (EGF), despite that their global protein backbones are still flexible [47].

Mfp-3 is a protein family normally located at the interface of the plaque and substratum, which is supposed to serve as an adhesive primer. Mfp-3 is a Dopa-rich protein which has the most polymorphic property and lowest molecular weight (5-7 kDa) [49]. There are about 30 different variants of Mfp-3 detected in the mussel plaque, which can be classified into two sub-categories named Mfp-3 *fast* (Mfp-3F) and Mfp-3 *slow* (Mfp-3S) [51, 53]. These two groups are defined based on the eluting fraction differences in reverse phase high-performance liquid chromatography

Table 1. Biochemical comparison of the DOPA-containing proteins of Mytilus species in the adhesive plaques and threads with regard to mass, pI, post-translational modifications, structure and localization in the foot glands and byssus [45].

Protein	Mass (kDa)	pI	Modifications (mol%)	Structure	Location	References
Mfp-1	~110	8-10	Dopa (10-15), Hyp	Disordered, PPII	Cuticle	13-16
Mfp-2	45	10	Dopa (5)	Disordered, EGF	Plaque core	15, 17
Mfp-3F	5-7	8-10	Dopa (7-20), HOArg	Disordered	Plaque interface	18-21
Mfp-3S	5-7	7-8	Dopa (8-14)	Disordered	Plaque interface	20- 23
Mfp-4	90	8.4	Dopa (2)	Disordered	Plaque core	24
Mfp-5	11	9.8	Dopa (30) pSer	Disordered	Plaque interface	25- 28
Mfp-6	12	9.3	Dopa (5)	Disordered, beta	Plaque interface	29
pCOL-D	240	9.5	Hyp; Dopa (0.1)	Collagen core, silk	Plaque, thread core (distal)	30-32
pCOL-P	240	9	Hyp; Dopa (0.1)	Collagen core, elastin	Plaque, thread core (proximal)	31-33
pCOL-NG	240	8.8	Hyp; Dopa (0.1)	Collagen core, glycine rich	Plaque, thread core	31, 32, 34
PTMP-1	50	5.9	Glycosylation	vWF fold	Thread core (proximal)	32, 35, 36
TMP-1	56.5	9.5	Dopa	Discordered	Thread core (distal)	32

PPII: polyproline II helix; EGF: epidermal growth factor; vWF: von Willebrand factor; HOArg: hydroxyarginine; Hyp: hydroxyproline; pSer: phosphoserine; pCOL-D, -P and -NG: prepolymerized collagens with distal, proximal and nongradient distributions; PTMP-1: proximal thread matrix protein1; TMP-1: thread matrix protein1

(HPLC), and are well separated on acetic acid urea polyacrylamide gels [71]. Other than Dopa, the main components of Mfp-3 are glycine (25-29 mol %) and asparagine (10-18 mol %). All the tyrosine residues in Mfp-3F undergo post-translation modification by mussels themselves to Dopa (17−20 mol %), while about half of this value is found in Mfp-3S (8−14 mol %). Additionally, the yield of Mfp-3S is more than twice that of Mfp-3F, and this is the most abundant directly extractable protein from the byssus plaques [51]. Mfp-3S is a key factor that enables the mussel adhesion by connecting the adhesion layer and other proteins in bulk of the plaque [54]. Moreover,

Mfp-3S is the first known adhesive protein which could perform self-coacervation naturally. Such self-concertation is a potential and likely crucial way for the delivery of adhesives.

Mfp-5 locates at the interface, and has the least polymorphic property compared to other plaque proteins [54, 56]. It has a low molecular mass (10 kDa), consisting of one protein sequence with two closely related variants. Containing the highest content of Dopa (30 mol %) residues, and large amounts of glycine amino acid (15 mol %) and lysine amino acid (17 mol %), Mfp-5 serves as an important adhesive primer at the plaque interface, showing the highest adhesive energy (~ 14 mJ/m^2) among all the Mfps [66].

Mfp-6 is a thiol-rich protein that is assumed to mediate the redox of Dopa and the cross-linking of the interfacial proteins with those in the plaque by cysteinyl-Dopa bonds [72]. It is reported that Mfp-6 is rich in cysteine residues (11 mol %) with only a small ratio of cysteine residues bridging by disulfide bonds (2 mol %). It also contains a large amount of charged residues (16 and 23 mol% cationic and anionic amino acids, separately) but a low content of Dopa (typically less than 5 mol %) [56]. The most outstanding feature of Mfp-6 is to mediate the redox environment of the plaque. When Dopa are oxidized to Dopa-quinone at seawater pH with dissolving oxygen, the thiol residues in Mfp-6 is capable of reducing Dopa-quinone to Dopa, which maintains a reducing environment for the Dopa-rich proteins to preserve the strong adhesion to the target surface [72].

Byssus also composes of three divergent collagen proteins termed PCOLs, which are surrounded by matrix proteins. PCOLs are trimeric with secondary triple helical collagen cores flanked by silk-like β-sheets in PCOL-D and disordered elastin in PCOL-P and PCOL-NG [58]. The features of matrix proteins between the distal part and proximal part, as well as between proteins in the thread cuticle and the adhesive plaque, are significantly different. Several matrix proteins have been

clarified and reported before, but only limited to the presumption of their structures and functions. Proximal thread matrix protein1 (PTMP1) locates in the proximal portion of each byssal thread and controls the alignment of the collagen fibers in the byssus[62]. It is reported that PTMP1 binds to heterologous collagens via electrostatic attractions[73]. It is also reported that Zn^{2+}binds with the MIDAS motif of PTMP1, which enhances the collagen binding of PTMP1[73, 74].

2.2 Dopa Mediated Interaction in Mussel Foot Proteins

The Dopa-containing Mfps have been regarded as useful design models for the development of synthetic polymers with various applications, such as wet adhesives [1, 49, 51, 66, 75, 76], antifouling coatings [77, 78], magnetic imaging agents [79], tissue glues [24], surface modification [80] and pH-sensitive hydrogels [81]. The most distinctive characteristic of Dopa in mussel protein adhesives is to mediate various interactions on different types of substrates, including bidentate hydrogen bond [9, 82, 83], metal-catechol coordination bond [84, 85], π–π/π-cation interactions [85-87], oxidative cross-linking [2, 88, 89] and electrostatic interaction (Fig. 2). Many of these interactions have been identified using the surface forces apparatus (SFA) technique [90]. Since the interactions of Dopa with different substrates play essential roles in the properties and functions of Mfps and mussel-inspired adhesives, we highlighted the Dopa-medicated interactions in several as-known adhesive proteins in this work.

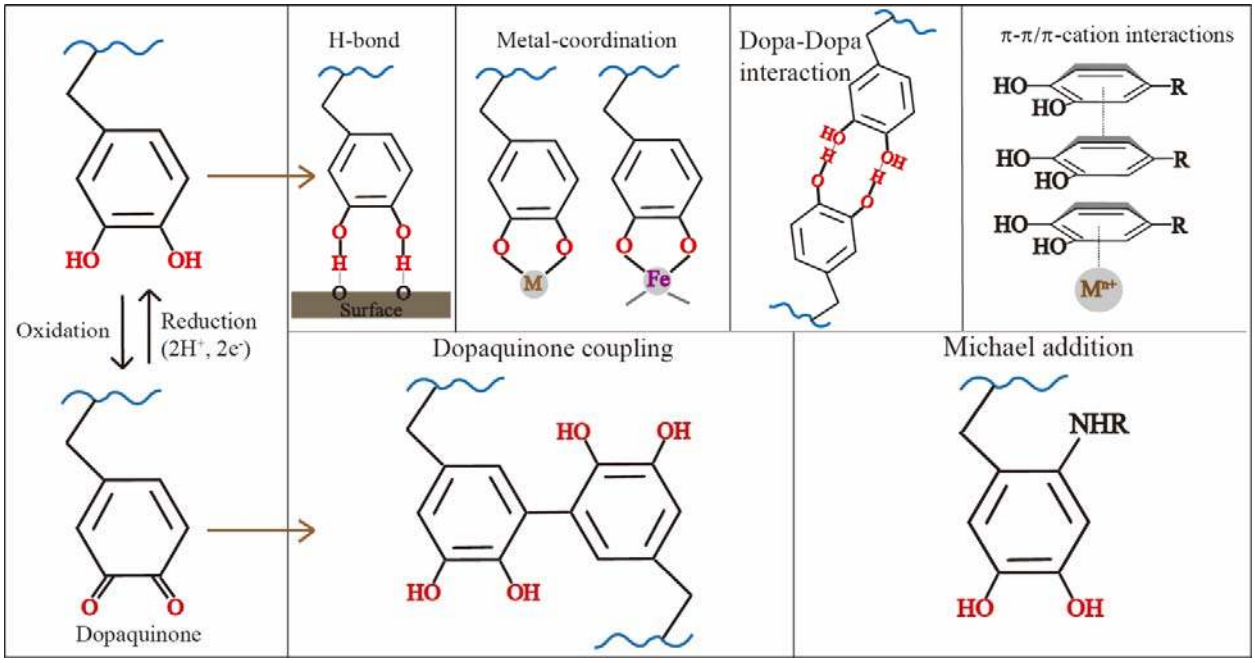

Fig. 2 Schematic illustration of various interaction and reaction products with Dopa

Recently, various studies on the adhesive proteins Mfp-3 and Mfp-5 have elucidated the critical role of Dopa in the mussel wet adhesion system, where bidentate hydrogen bond [4, 9] and metal coordination bond [91] are recognized as the major factors that contribute to the adhesive properties of Mfps. Bidentate hydrogen bond is proposed to be responsible for the adhesion of Mfp-3F on hydrophilic substrates such as mica and other mineral surfaces [92]. Although a single hydrogen bond is relatively weak, forming a bidentate hydrogen bond can dramatically increase the lifetime of the bond by 10^6 times, providing the Dopa residues strong ability to adhere to diverse hydrophilic surfaces [90]. Within the Mfps, Dopa facilitates the strong cohesion by forming Dopa-Dopa bidentate hydrogen bonds [93]. Dopa-metal coordination bonds play critical roles in the adhesion of Mfps on metal oxide surfaces [9]. Studies on Mfp-3 reveals a pH-dependent binding mechanism on TiO_2 surfaces that involves both bidentate hydrogen bonding at a low pH environment and coordination bond at elevated pHs (pH > 7). Raising the pH of the medium can

promote the forming of bidentate Dopa-Ti coordination bond, resulting in a further stabilization of the Dopa and thereof an increment in adhesion force [9].

Dopa-metal complexes also contribute to the mechanical integrity of mussel adhesive plaques. The Dopa-Fe^{3+} coordination complexes can provide extensibility, hardness, and self-healing features to the protective coatings which cover the exposing surfaces of byssus[94, 95]. It is reported that Mfp-1 located at the cuticle can form various complexes with Fe^{3+}, including bis- and tris- forms, owing to the high binding and stability constants of the catechol-Fe^{3+} coordination complexes[91, 94]. Recently, the Dopa-Fe^{3+} complexation has been investigated using Mfp-3F, and the results reveal that under low pH environment close to the local acid environment where the adhesive proteins are secreted, intrinsic strong surface adhesion dominates, and then strong cohesion occurs under higher pH close to the seawater environment mediated by the Dopa-Fe^{3+} complexation [91].

Interestingly, the oxidative cross-linking has been detected for the thiol-rich Mfp-6 [2, 56]. At the pH of 8.2 where Dopa residues can be readily oxidized, 5-S-Cysteiny-lDopa was identified with the amount of nearly 1 mol %. These reports indicate that Mfp-6 can create a cohesive bonds between the surface-coupling Dopa-rich Mfps and the plaque proteins [56]. In another research, the authors also demonstrate that during adhesive plaque formation, mussels can retard Dopa oxidation by exposing itself to an acidic, reducing environment with the existence of the thiol-rich Mfp-6, which protects Dopa by the combination of half reactions, the oxidation of thiols and reduction of Dopaquinone [2].

The report on the cation-π and π-π interaction involved in the mussel adhesive proteins have pictured a complementary cross-linking mechanism critical to the underwater adhesion of the Mfps [86, 87]. The interaction between the aromatic ring of catechol and other aromatic groups can be

enhanced by the π-π interaction, which contributes to the adhesion of Mfps on surfaces rich in aromatic components (e.g., PS) [96]. Recently, the possible synergistic relationship between Dopa and cationic amino acids is reported[97, 98]. Short-range cation-π interaction is generated when aromatic groups interact with positively charged residues, like lysine and arginine, and has been recognized as an important non-covalent interaction. For example, strong cohesion of mfp-1 were measured at pH 3, which was mainly attributed to the cation–π interactions [87]. Similarly, the robust adhesion and cohesion of pvfp-1 was demonstrated to be induced by cation–π interactions between Lys and 7OHManTrp and structural conformation changes, providing a promising approach to the design of novel bio-adhesives with effective underwater adhesion [86]. For Dopa-rich and Lys-rich mussel foot proteins, cation- π interaction can greatly contributes to the cohesion of the Mfps. Besides Dopa, other aromatic amino acid residues, such as phenylalanine (Phe) and tyrosine (Tyr), can also contribute to the strength of cation-π interaction[98, 99].Additionally, positively charged residues, like lysine and arginine, show synergy effect with Dopa residues in Mfp-3 and Mfp-5 on negatively charged surfaces, such as mica and many other mineral surfaces, via electrostatic interactions[4, 100].

2.3 Effect of pH

The mussels normally adapt to the seawater habitats with the pH values around 8. Since Dopa tends to be oxidized in neutral and basic pH [101, 102], the pH of the local environment has strong influences on the Dopa interaction mechanisms and the properties of the Mfps and mussel-inspired adhesives [90, 103-107].

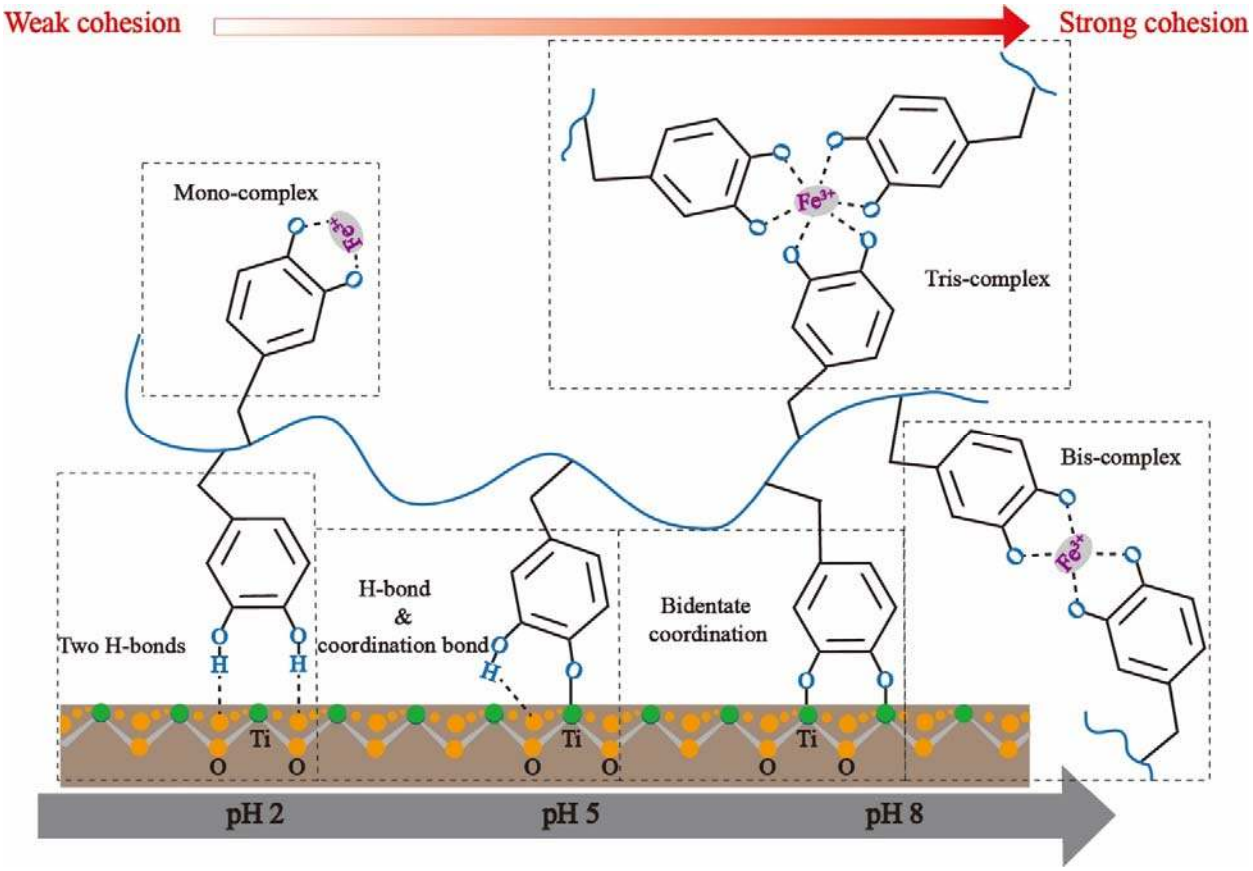

Fig. 3 The pH dependence of plaque chemistry. The coordination between metal ions and Dopa increases in valency from no cross-linking at low pH (cohesion is very weak) to three at pH ~8 (strong cohesion). Interfacial Dopa bonding of TiO_2 surfaces changes from hydrogen bonds at low pH to bidentate coordination bonds at pH 8. Reproduced with permission [91]. Copyright© 2016 American Chemical Society

At different pHs, Dopa can form stoichiometric mono-, bis-, and tris-complexes with Fe^{3+} in solution (Fig. 3) [91]. It is reported that the pH required to form the bis- and tris-complexes of Dopa-Fe^{3+} coordination is typically in the basic range [8, 9, 11]. Recently, an original method, which mimics mussel's byssus formation process, has been developed to form Dopa-Fe^{3+} polymer cross-links at basic pH to avoid Fe^{3+} precipitation [44, 81, 91]. Another study on Dopa-boronate complexation indicated that the complex could be formed at pH 9 but absent when pH decreased to 3. The nature

of the catechol−boronate complex enabled the reversible transformation of adhesives between its adhesive and non-adhesive forms with the change of pH.

The hydrogen bonding of Dopa to various substrates is also pH dependent [45]. On metal oxides surfaces, the bonding of Dopa can be tuned from the bidentate hydrogen bonding to bidentate-binuclear coordinative bonding (Fig. 3); in the process, one catechol group firstly forms two hydrogen bonds with the surface at pH ~ 3, followed by one hydrogen bond and one coordination bond at pH ~ 5, and finally two coordination bonds at pH ~8 [9, 104, 105, 108, 109].

2.4 Interactions of Mussel Adhesive Proteins on Different Substrate Surfaces

The marine mussels can establish robust attachment to various surfaces through the Dopa-containing mussel foot proteins. The adhesion strongly depends on the features of the contacting surfaces, solution environment, the bulk deformation and the bonding/debonding mechanics [110]. In this session we will briefly summarize the adhesion of Dopa-containing Mfps to various substrates. The binding mechanism of Dopa to metal oxide surfaces have been discussed in the previous session and therefore not covered here.

Mica is a hydrophilic, negatively charged aluminosilicate mineral and its exposed surface in water is polysiloxane with minor replacement of Si by Al (Fig. 4a). Mica is used as a popular substrate in the investigation of mussel adhesive proteins due to its atomically smooth basal plane, which is needed in the SFA measurements. Dopa can form bidentate hydrogel bond on mica surfaces as the distances between adjacent O atoms on mica (0.28 nm) matches with the distance of the two OH groups of Dopa (0.29 nm) [19, 111, 112]. Among all the Mfps tested, Mfp-5 consisting of the highest Dopa content demonstrates the strongest adhesion to mica when absorbed on the surface and

compressed at low pH [85]. As mica is negatively charged, electrostatic interactions between the positively charged amino acid residues in the Mfps (e.g. lysine) and mica also contributes to the adhesion of the proteins to mica surfaces [90, 113].

The interaction of Mfps with SiO_2 (Fig. 4c) is similar to that on mica surfaces, in which bidentate hydrogen bonding by Dopa dominates and the electrostatic interactions also play a role. For Mfp-3 in particular, the contact time dependence of the adhesion is stronger on SiO_2 substrate than that of mica surface, with a proportional relationship [85], which is most likely ascribed to the high surface roughness of SiO_2. Unlike Mfp-3 and Mfp-5, the adhesion of Mfp-1 to SiO_2 substrate was lower than that of mica surface. Such results may be due to the higher chain flexibility and smaller molecular weights of Mfp-3 and Mfp-5 to fit better to the interfacial roughness of SiO_2 than Mfp-1 [8].

It is known that when solid surfaces are exposed to seawater or physiological fluids, they will be fouled by biomolecules within only a few minutes [10]. Therefore, the adhesion of various Mfps on organic surfaces have been extensively studied. The adhesion of Mfps on organic surfaces has been conducted using organic thin films (Fig. 4b). At acidic pH, the strong adhesion forces were measured between various Mfps (Mfp-1, Mfp-3, and Mfp-5) and methyl-terminated self-assembled monolayers (SAMs) on atomically smooth gold substrates due to the hydrophobic interactions [10].

Mfps can form the hydrogen bonding and hydrophobic interactions to PMMA (Fig. 4d). On PMMA, the most hydrophobic protein, Mfp-3S, exhibits the highest adhesion force compared with Mfp-1 and Mfp-5, while Mfp-1 and Mfp-5 show similar values of the adhesion force. [51] The hydroxyl and amine groups on Mfps can form hydrogen bonds with the acrylate groups of PMMA,

while the hydrophobic interactions occur between the alkyl part of PMMA and the hydrophobic amino acid residues on Mfps [8, 110].

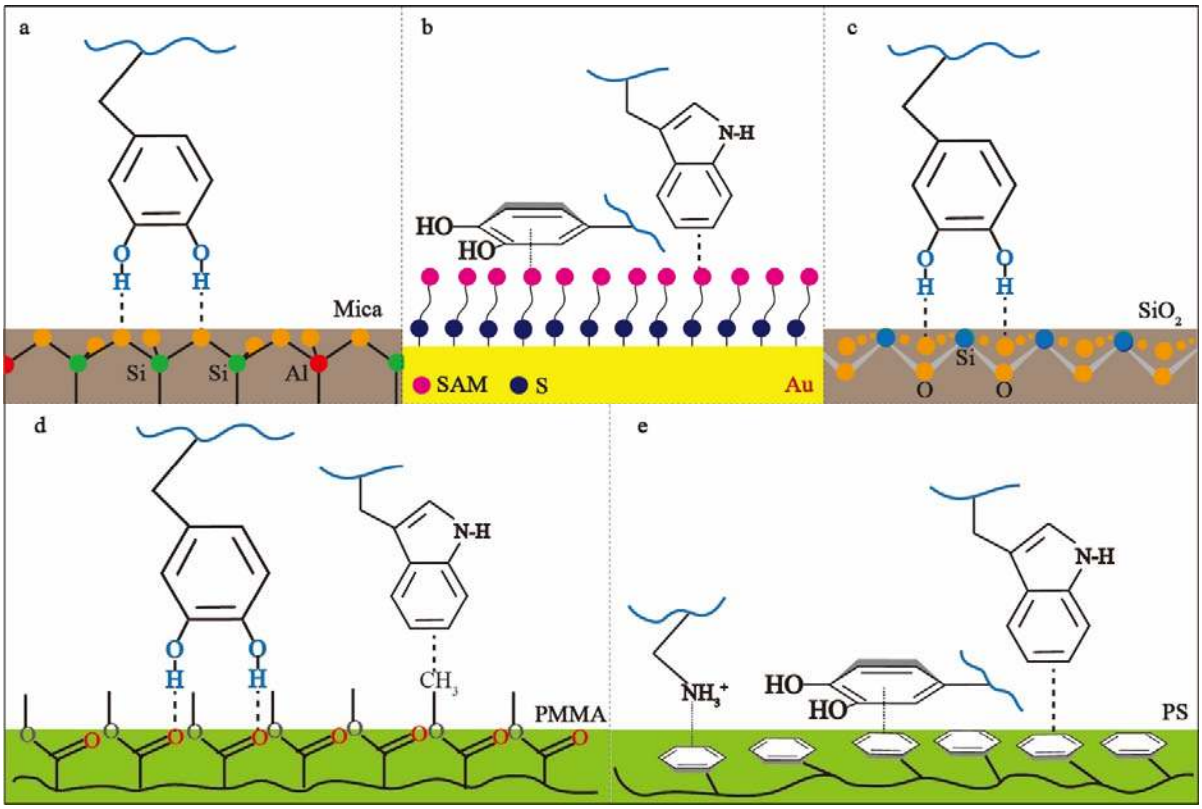

Fig. 4 Dopa can form (a) bidentate hydrogen bonds on mica surface; (b) hydrophobic interactions on organic thin films; (c) bidentate hydrogen bonds on SiO_2 surface; (d) bidentate hydrogen bonds and hydrophobic interactions on PMMA surface; (e) cation-π interactions, π–π interactions and hydrophobic interactions on PS surface.

Hydrophobic, cation-π and π–π interactions are critical for the adhesion between Mfps and polystyrene (PS) (Fig. 4e) [8, 86, 114, 115]. Strong adhesion was measured within an extremely short contact time (i.e. 2 min) for Mfp-3 and PS substrate. Similar to PMMA surface, the hydrophobic interactions can originate from the hydrophobic amino acid residues in Mfp-3 and PS. The cation–π interaction is mainly due to the positively charged residues, like amides in the Mfp-3 and benzene

groups on PS. Besides, aromatic groups in Mfp-3 interact with the benzene groups through π–π interaction.

III MUSSEL-INSPIRED SYNTHETIC POLYMERS

3.1 Coacervate Dopa-Functionalized Adhesives

During the liquid protein adsorption process, mussel foot proteins exist as the form of coacervates[51]. Coacervation is the liquid-liquid phase separation of a colloidal system consisting of ionic polymers or proteins [116], and the dense fluid of concentrated polymers referred to as a coacervate plays an important role in the outstanding wet adhesion of marine organisms such as mussels and sandcastle worms [1, 117]. For the well-studied Mfp-3S, it forms self-coacervation and it is driven by both electrostatic attraction and hydrophobic interaction[51]. Recent study also reveals that PCOLs can form confined a liquid crystal phase in the vesicles and this liquid phase could be harnessed into continuous birefringent fiber in the byssus formation process[118]. The formation of the coacervate is generally driven by weak and nonspecific interactions including electrostatic attraction, hydrophobic interaction and hydrogen bonding, followed by the entropic gains by releasing of ions and water molecules, [119-121] which is susceptible to the solution and environmental conditions (e.g., concentration, pH, ionic strength) [122, 123]. Taking advantage of their relatively high viscosity, reduced interfacial energy and high diffusion coefficients of the solute and solvent molecules, the Dopa-functionalized coacervates with great wetting properties and adhesiveness have become promising candidates as effective underwater adhesives [6].

Complex coacervation resulting from the neutralization of two oppositely charged polyelectrolytes has been thoroughly investigated since it was firstly systematized by Bungenberg de Jong (Fig. 5a)

[124]. Stewart et al. developed water-borne adhesives mimicking the sandcastle worm glue, where Dopa-containing polyphosphate and poly-aminated gelatin formed complex coacervates at the specific pH and ionic strength [117, 125]. The coacervates showed great potential as bone adhesives, in which the Dopa residues not only facilitated the strong underwater adhesion but also hardened the adhesives by covalent crosslinking. To improve the bulk setting and adhesion of the coacervates, a polyelectrolyte complexation was developed by solvent exchange from a dimethyl sulphoxide (DMSO) solution of catechol-functionalized poly(acrylic acid) and quaternized chitosan [126]. When the solution was applied underwater, coacervation, phase inversion, setting and solidification were rapidly induced (~25 s), and the synergy between electrostatic complexation and catechol chemistry resulted in a microporous adhesive showing robust underwater adhesion on various substrates. Mussel adhesive proteins are also exploited for coacervation, and since all the identified Mfps are positively charged under physiological conditions[1], an anionic polysaccharide hyaluronic acid (HA) has been successfully employed to form complex coacervates with various cationic recombinant Mfps, exhibiting superior spreading and adhesive properties. Cha and coworkers prepared large quantities of recombinant Mfps (fp-151, mfp-151, fp-131 and mfp-131) and investigated their ability to form complex coacervates with HA in the pH range of 3.0-4.6 [15]. The optimal mixing ratio of Mfp to HA was found to be 8:2 (wt/wt) confirmed by the droplet-like morphology, and the successful microencapsulation of oil particles within the coacervates suggested their great potential in drug delivery applications. Interestingly, although no adhesion could be detected in non-coacervated mfp-151 in the wet environment, the mfp-151/HA coacervates showed a relatively good underwater adhesion of 0.24 MPa with aluminum due to the increased density of adhesive proteins. Hwang and coworkers examined the flow behaviors of Dopa-containing fp-151-RGD/HA coacervates with the help of a surface force

apparatus (SFA) [14]. With the mixing ratio yielding maximum coacervation, the coacervate exhibited shear-thinning viscosity and extremely low interfacial energy with water (< 1 mJ/m^2), which favored the spreading of the coacervates over surfaces, and the high friction coefficient (> 1.2) indicated the further slippage of the wet adhesives was prevented. The wear protection capabilities and mechanisms of coacervates to surfaces were thoroughly investigated by shearing mfp-1/HA complex coacervates between two mica surfaces using the SFA [23]. Without Dopa functionality, the coacervates lacked the stable attachment to surfaces, leading to surface damage under low applied load, while in the presence of Dopa, the enhanced adhesion between coacervates and surfaces would shift the slip-plane up from the surface into the intervening coacervate layer, significantly improving the wear protection capability by 5-fold. Recently, a zwitterionic protein rmfp-3b was reported to form upper critical solution temperature (UCST) mediated complex coacervates with citrate at pH 3.0, and the transition temperature could be easily adjusted between 2 ºC to 16 ºC with different citrate and protein concentrations [127]. The UCST behavior was attributed to the reduced hydrophilicity of proteins and deprotonation of citrate at low temperature, which inspires the development of novel coacervated adhesives with thermo-responsiveness. In addition to the aforementioned polycation/polyanion complex coacervation, Kim et al. reported a complex coacervate formation from two positively charged polyelectrolytes as indicated in Fig. 5b [22]. The like-charged coacervation was driven by short-range cation–π interaction[85] between aromatic phenolic groups in rmfp-1 and cationic groups in poly(2-(trimethylamino)ethyl methacrylate, which was strong enough to overcome electrostatic repulsion.

Self-coacervation involves only a single polyelectrolyte for coacervate formation and was demonstrated by zwitterionic and hydrophobic Mfp-3S (Fig. 5c) [128]. The phase separation of Mfp-3S was largely dependent on the pH and ionic strength, suggesting both electrostatic attraction

between basic and acidic residues and hydrophobic interactions contributed to the protein coalescence. Taking advantage of Mfp-3S's unique capacity to self-coacervate and increase the oxidation potential of Dopa [129], a series of Mfp-3S-mimetic copolymers were prepared for the

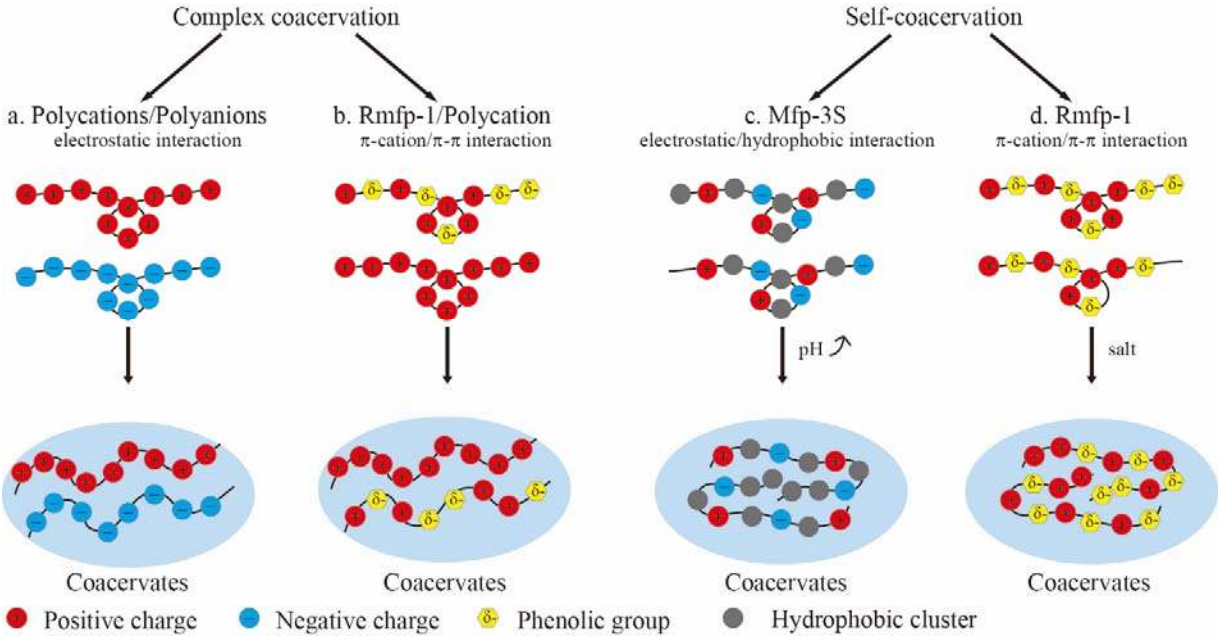

Fig. 5 Schematic representation of different coacervation systems. (a) Complex coacervation formed between oppositely charged polyelectrolytes. (b) Like-charged complex coacervation facilitated by short-range cation–π interaction. (c) Self-coacervation formed by zwitterionic and hydrophobic Mfp-3S with increasing pH. (d) Self-coacervation of cationic and polyphenolic rmfp-1 with increasing salt concentration. Reproduced with permission [51]. Copyright © 2013, COMPANY OF BIOLOGISTS LTD

development of coacervated adhesives, which consisted of catechol functionality, ionic (cationic and anionic) and amphiphilic (nonionic hydrophilic and nonionic hydrophobic) groups [52]. By optimizing the hydrophilic/hydrophobic as well as cationic/anionic ratios, the developed ampholytic copolymer exhibited stable coacervation and strong wet-cohesion (~32.9 mJ/m^2) which was 9 times higher than that of native Mfp-3S. Moreover, a Dopa-containing peptide (mfp3S-pep) was designed in order to investigate the effect of Dopa on coacervation and adsorption of the peptide on bio-related surfaces such as TiO_2 and hydroxyapatite (HAP) [4].

Although Dopa only showed slight influence on coacervation, it was indispensable for promoting peptide adsorption by removing interfacial water from the target surfaces. Waite and coworkers developed a simple wet adhesive primer from low-molecular-weight catecholic zwitterionic surfactants compromising amine, phosphate, hydrophobic and catechol functionalities[130]. The coacervated zwitterionic platform with reduced complexity offered smooth and thin coatings (< 4 nm) on various substrates with strong wet adhesion up to ~50 mJ/m^2, implicating great promise for nanofabrication. Besides zwitterionic systems, self-coacervation occurred in cationic and polyphenolic rmfp-1 (Fig. 5d), which was attributed to strong cation−π interaction at short range[131]. The coacervate formation was triggered by salt concentration similar to nature seawater condition (> 0.7 M), since salt screened the electrostatic repulsion while still maintained the attractive cation−π interaction. The friction coefficient (< 0.03) of the formed coacervate was remarkably lower than that of conventional coacervates, expanding their applications as lubricants.

3.2 Adhesive Hydrogel

As highly water-swollen three-dimensional networks, hydrogels possess structural resemblance to biological tissues and high permeability to oxygen and nutrients, which have been designed as platforms for diverse biomedical applications such as drug delivery, tissue engineering and implantable devices [132, 133]. Particularly, intense efforts have been spent on the development of adhesive hydrogels with biocompatibility and sufficient wet adhesion, holding considerable promise as tissue adhesives to replace surgical sutures and tapes for wound management [134]. Owing to the robust adhesion and cohesion of Mfps in wet conditions, hydrogels functionalized with Dopa

and its analogues have aroused great interest as a new family of tissue adhesives over the past two decades [20].

Poly(ethylene glycol) (PEG) is one of the most widely-used synthetic polymers for the development of hydrogels with outstanding hydrophilicity and biocompatibility, and the Messersmith group has incorporated Dopa or catechol functionality as terminal or side groups to a family of PEG polymers with different structures (e.g., linear, hyperbranched, and block) [135-137]. The *in vivo* performance of the catechol-modified PEG adhesive hydrogel was further investigated, where the in-situ gelation was induced within 1 min by oxidation and the transplanted islet was immobilized on the extrahepatic tissues up to one year with minimal inflammatory response[138]. When an Ala-Ala dipeptide substrate was incorporated between the catechol group and the branched PEG, the adhesive hydrogel displayed enzymatic degradation upon the addition of neutrophil elastase over several months, showing improved cellular infiltration after dorsal subcutaneous implantation in mice [24]. A facile synthesis of injectable bio-adhesives (iCMBA) based on PEG, citrate and Dopamine was reported by Yang et al., and the adhesives displayed strong adhesion to wet tissue surfaces with 2.5–8.0 folds higher strength than that of fibrin glue [139]. Multi-functionality was demonstrated in the system, including tissue-like elastomeric behavior, capability to stop bleeding and facilitate wound healing, biocompatibility and degradability. Furthermore, the adhesive iCMBA was composited with HA to serve as an injectable implant for the treatment of comminuted bone fractures [140]. The addition of HA significantly enhanced the mechanical strength and bio-mineralization process of the hydrogel without sacrificing adhesiveness, promoting neovascularization and bone formation *in vivo*. A highly branched PEG hydrogel was rendered wet adhesion by copolymerization with catechol-derived monomers [141]. The mechanical strength and adhesion could be conveniently controlled by UV radiation that

modulated the crosslinking density, and the thermo-induced shrinking of the hydrogel not only avoided the mechanical weakening underwater but also expanded their practical application as smart drug carriers.

Owing to their outstanding biocompatibility and biodegradability [142], naturally occurring polymers, especially polysaccharides, have been extensively explored for the development of injectable adhesive hydrogels in combination with Dopa derivatives. Catechol-modified HA [143] and chitosan [144] were mixed with thiol-terminated Pluronic F-127, generating viscous solutions via Michael-type catechol-thiol addition reaction. Taking advantage of the thermo-responsiveness of Pluronic, the sol-gel transition could be rapidly triggered at body temperature after injection. The redundant catechol units imparted the HA/Pluronic and chitosan/Pluronic with strong adhesive strength to soft tissues of 7 kPa and 15 kPa, respectively. Catechol-conjugated alginate [145] and HA [146] hydrogels prepared by oxidative catechol polymerization exhibited low immunogenicity and no cytotoxicity, and the cell-containing HA-catechol adhesive was successfully utilized for minimally invasive cell therapy showing improved therapeutic and regenerative capacity of transplanted cells. To simplify the preparation process of Dopa-containing polymers, Cho and coworkers reported an enzyme-mediated biosynthesis method which converted the tyrosine residues on extracted human gelatin into Dopa [147]. The Dopa-modified gelatin was crosslinked upon addition of Fe^{3+} through Dopa-Fe^{3+} complexation, where the hydrogel maintained the stability underwater and showed adhesion to a rat liver with hemostatic ability. The poly(γ-glutamic acid) grafted with Dopamine (with a 36.5% degree of substitution) could lead to an injectable hydrogel via enzymatic crosslinking method, displaying extremely strong adhesion to wet tissues of 58.2 kPa which is 10–12 times higher than fibrin glue [148]. Since the consumption of catechol groups during metal

coordination or oxidation for gel formation generally undermines the adhesive property of the

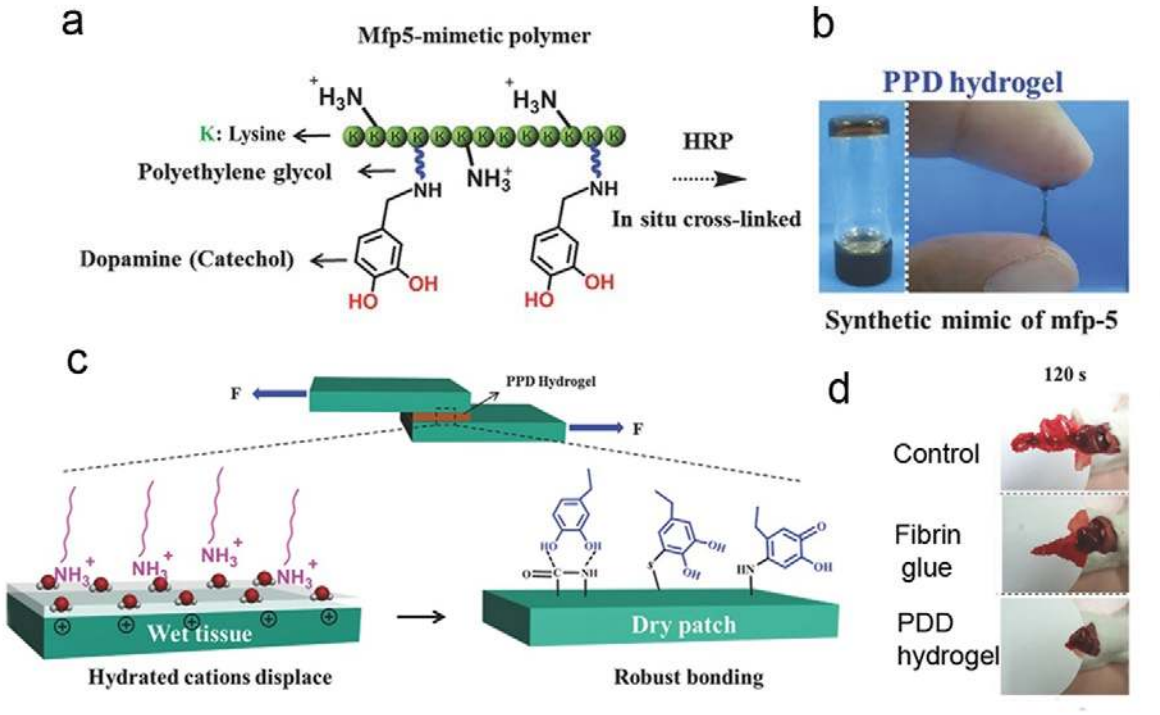

Fig. 6 A mussel-inspired adhesive hydrogel (PPD). (a) Mfp-5 mimetic polymer formation from Dopamine and ε-poly-L-lysine. (b) Preparation of PPD hydrogels through a HRP crosslinking reaction. (c) Schematic illustration of the lap-shear test and the proposed mechanisms of the catechol–Lys cooperative effect for the enhanced wet adhesion. (d) Bleeding level of the damaged mouse liver treated with PPD hydrogel, fibrin glue, and untreated after 120 s. Reproduced with permission [149]. Copyright © 2017, Wiley–VCH, GmbH & Co. KGaA

mussel-inspired hydrogels, Schiff base reaction was employed for the crosslinking of an injectable hydrogel from hydrazide-modified poly(γ-glutamic acid) and dual (i.e. aldehyde and catechol)-functionalized alginate [150]. With a large number of preserved catechol units, the unoxidized hydrogel maintained the strong adhesion after several attachment-detachment cycles due to the reversible interactions between catechol moieties and the substrates. Adhesive hydrogels based on a Dopa-containing recombinant Mfp-1 were developed via both Fe^{3+}-mediated noncovalent and quinone-mediated covalent crosslinking [151]. Fe^{3+}-crosslinked hydrogel was deformable with a bulk

adhesion to porcine skin up to ~130 kPa, while the quinone-crosslinked hydrogel via oxidation showed enhanced mechanical strength and stronger wet adhesion of ~200 kPa. Recently, Xu et al. reported an Mfp-5 analogue hydrogel (PPD) for wound management with robust wet adhesion (147 kPa) provided by a cooperative effect between catechol and lysine residues [149]. As shown in Fig. 6, when the hydrogel was applied on soft tissues, the cationic amines of lysine would displace hydrated cations from the wet surfaces, leading to a drier patch for catechol cohering with the nucleophiles of biological molecules. The outstanding bio-adhesion endow the hydrogel hemostatic capacity to accelerate wound healing and tissue regeneration, and the anti-infection property was also integrated into the multifunctional hydrogel due to the inherent antibacterial ability of ε-poly-l-lysine.

Although soft adhesive hydrogels with injectability offer unique advantages of easy administration and minimal invasion [152], they usually suffer from poor mechanical properties and short-term stability. Therefore, tough hydrogels with sufficient mechanical strength and adhesiveness have drawn considerable attention as strong tissue adhesives. Nitro-Dopamine methacrylamide and 3-acrylamido phenylboronic acid were conjugated in a polyamide hydrogel to enhance its interfacial adhesion as well as bulk cohesion [153]. The excellent mechanical strength (toughness of 590 J/m^2) was mainly ascribed to the formation of dynamic boronate ester bond, and the high adhesion energy (> 400 J/m^2) was contributed by a faster quinone–nucleophile coupling of nitro-catechol with tissue surfaces, compared to unmodified catechol groups. Incorporating nanoparticles into hydrogels have been demonstrated to improve the performances of the materials, and N-hydroxysuccinimide modified poly(lactic-co-glycolic acid) (PLGA) nanoparticles (PLGA-NHS) were blended with alginate–Dopamine polymer (Alg-Dopa) to enhance its adhesiveness to 33 kPa from 14 kPa of Alg-Dopa hydrogel alone [154]. An ultra-tough double-network hydrogel was formed

by Dopamine-grafted oxidized sodium alginate (OSA-DA) and polyacrylamide (PAM) through Schiff base reaction and hydrogen bonding interaction [25]. The chemically and physically crosslinked network possessed a high tensile strength of 109 kPa and ultra-stretchability of 2550%, with proper adhesiveness to various substrates and excellent cell affinity.

In addition to hydrogels developed from catechol-functionalized polymers, Lu and coworkers reported a general approach to tough and adhesive hydrogels by facilely introducing poly-Dopamine (PDA) into hydrogel networks [155]. As illustrated in Fig. 7a and b, PDA polymerization was induced in alkali solutions, where overoxidation was prevented to maintain sufficient free catechol groups for tissue adhesion. After free radical polymerization of acrylamide monomers dispersed in PDA solution, a PDA-PAM hydrogel with a super stretchability (3300%) and a high fracture energy (2400 J/m^2) was generated due to the great balance between non-covalent interactions (i.e. hydrogen bonds, π–π stacking, hydrophobic interactions) and covalent bonds in the hydrogel. The oxidation of Dopamine could also be triggered by clay, and the resultant PDA was confined between the clay nanosheets [156]. The nanocomposite hydrogel displayed good adhesion to various substrates including glass, metal, plastics and tissues. It is worth mentioning that the 28.5 kPa adhesive strength of the hydrogel to porcine skin could be completely maintained even after 20 cycles of peel-off test. The universal platform was further explored to produce multifunctional hydrogels. When graphene oxide was introduced to the PDA solution, it would be partially or fully reduced, rendering the hydrogel high conductivity in combination with the toughness and adhesiveness for applications in motion sensing [156]. Besides, A transparent, conductive and adhesive hydrogel was developed by oxidizing Dopamine and pyrrole molecules together, which gave rise to conductive PDA−PPy nanofibrils in the network, holding great promise as transparent electronic skin and smart implantable devices [26]. Inspired by algae and

mussel, a simple combination of PDA, alginate, and Fe^{3+} ions could also form adhesive hydrogels. The adhesive hydrogels exhibited a high tensile adhesive strength of 400 kPa and a high tolerance towards humidity gradually got hardened. [157] Very recently, a conductive and adhesive PDA-CNTs based hydrogel was designed. DA was polymerized on carbon nanotubes (CNTs) to form uniformly dispersed PDA-CNTs, and then acrylamide (AM) monomers, acrylic acid (AA) monomers and glycerol were added. By UV-initiated copolymerization, the GW-hydrogel was generated. The hydrogel could maintain normal mechanical properties under extreme temperature conditions (from -20 ºC to 60 ºC). It exhibited tissue adhesiveness of 60 kPa, high stretching ability of 700%, great toughness of 2300 Jm^{-2} and excellent recoverability generated from the noncovalent interactions.[158]

As a natural polyphenol, tannic acid (TA) involves five pyrogallol and five catechol groups [159], and it was employed for the preparation of wet adhesives with hemostatic property by simply mixing it with PEG solution [160]. Jin et al. developed a TA-based polyphenol hydrogel with cationic poly(dimethyl diallyl ammonium chloride) (PDDA) showing both strong cohesion and adhesion (Fig. 7c and d) [161]. Owing to the high density of pyrogallol/catechol groups of TA, the high crosslinking density via noncovalent interactions (e.g., ionic interactions, hydrogen bonding, and coordination with Fe^{3+}) endowed the hydrogel enhanced cohesion, and simultaneously, the acidic condition prevented the oxidation of TA functional groups, which guaranteed the robust adhesion to diverse substrates. Combining TA with poly(vinyl alcohol) led to a dual-cross-linked hydrogel with superior mechanical strength (e.g., tensile strength of 9.5 MPa, elongation of 1000% and adhesiveness over 70 kPa), which was mainly attributed to multiple hydrogel bonds provided by TA [162]. When TA-coated cellulose nanocrystals were incorporated into ionic hydrogels, the

dynamic coordination bonds formed with TA contributed to the excellent mechanical property, self-healing ability and repeatable adhesiveness of the system [163].

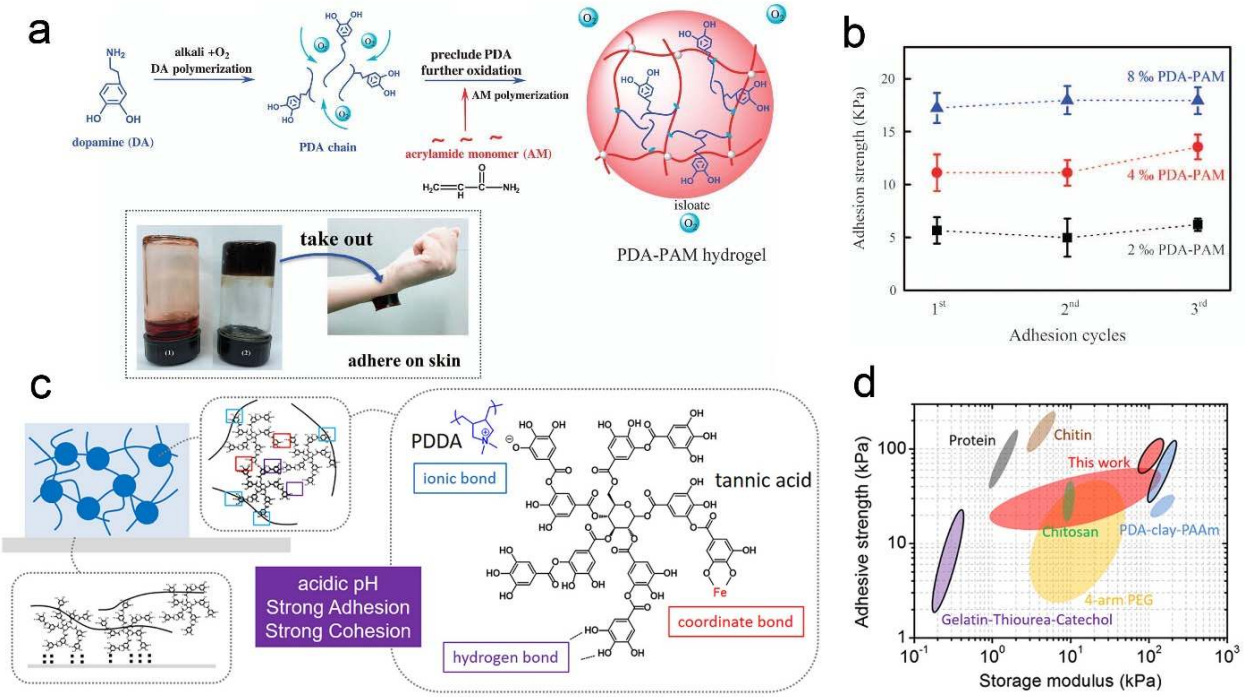

Fig 7. (a) Schematic representation of the two-step formation of PDA-PAM hydrogel from Dopamine polymerization and free radical polymerization. Photo: the prepared hydrogel firmly adhered to human skin. (b) Reversible adhesion of the PDA–PAM hydrogels to porcine skins over attachment-detachment cycles. Reproduced with permission [155]. Copyright © 2017 Nature Publishing Group (c) Schematic illustration of the TA-based PDDA hydrogel with abundant pyrogallol/catechol groups. (d) The comparison of the storage modulus and adhesive strength of the prepared TA-based hydrogel with other reported catechol-based hydrogels. Reproduced with permission [161]. Copyright © 2017 American Chemical Society

The various physical and chemical interactions offer by catechol groups have been utilized not only for wet adhesion but also for the design of self-healing hydrogels. The reversible coordination between Mfps and metals have inspired the development of a series of self-healing hydrogels by mixing catechol-functionalized 4-arm PEG with a variety of trivalent metal ions (i.e. Fe^{3+}, V^{3+}, Al^{3+}) [81, 164]. The formation of mono-, bis- and tris-catechol-metal complexes could be finely tuned

by the pH of the environment, and the viscoelastic properties of the material were facilely modulated over several orders of magnitude by the selection of solution condition as well as metal ion identity. Similarly, catechol functionality was integrated into polymers containing amine groups such as polyallylamine and chitosan, and self-healing hydrogels were generated upon coordinating with Fe^{3+}, Al^{3+}, Ga^{3+} and In^{3+} around physiological pH [27, 165]. Since the oxidation of catechol groups plays a critical role in the mechanical strength and self-healing property of the hydrogels, Birkedal and coworkers reported a catechol-based hydrogel with controlled oxidation degree by employing two kinds of catechol analogues, where the oxidation-resistant moieties formed reversible coordination bonds with Fe^{3+}, and the oxidation-sensitive units generated covalent crosslinks. Thus, both mechanical stiffness and self-healing property were achieved and could be conveniently modulated [166]. When chitosan was modified with nitro-catechol, the catechol–Fe^{3+} complexation permitted self-healing ability in an extremely strong and stiff polymer (with an elastic modulus of 862 MPa) [167]. Catechol-boronate complexation was also exploited to design pH-responsive hydrogels with self-healing properties due to the dynamic nature of the boronate ester linkages. As phenylboric acid was able to form phenylborate ester with other vicinal diols in addition to catechol units, the hydrogels based on phenylborate esters were demonstrated to display responsiveness to monosaccharide such as glucose, galactose, and fructose [168, 169]. However, most hydrogels based on boronate esters were formed at pH > 8 due to the high pK_a, and recently, a self-healing and biocompatible hydrogel was developed via benzoxaborole-catechol complexation, in which the gelation easily occurred in at physiological pH (7.4) [170]. In a metal-free and acidic environment, self-healing ability was also evidenced in catechol-functionalized polyacrylate and polymethacrylate materials, which was mainly attributed to bidentate hydrogen bonding between catechol groups and facilitated by other physical interactions

[93]. Zeng et al. reported a thermo-responsive ABA tri-block copolymer consisting of catechol-functionalized poly(N-isopropylacrylamide) as A block and hydrophilic PEG as B block [171]. The rapid self-healing property of the injectable hydrogel was contributed not only by hydrogen bonding but also aromatic interactions (i.e. quadrupolar interactions and π–π stacking) between the catechol moieties. The antifouling property and biocompatibility of the hydrogel revealed its potential applications in biomedical fields. Following the same principle, when cationic poly[2(methacryloyloxy)ethyl trimethylammonium iodide] served as B block, the antibacterial performance to *E. coli* was imparted to the hydrogel with a combination of other aforementioned properties desired for bioengineering applications [172].

3.3 Smart Adhesives

Smart adhesives that can undergo on-demand bonding/debonding transition to substrates in response to external stimuli (e.g. temperature, pH, light) have gained growing interest for developing advanced functional adhesives, because the precise control of the adhesiveness is intriguing for numerous practical applications such as removable wound dressings, recyclable packaging and reusable structural components [173-175]. Mussel-inspired smart adhesives have been generated taking advantage of the strong wet adhesion of Dopa and the responsiveness of catechol chemistry.

Enzyme-activated adhesives were developed from Mfp-derived peptides containing tyrosine residues, where the adhesive state could be switched on from the non-adhesive state by tyrosinase [31]. Single molecule force spectroscopy revealed that the binding force of per peptide molecule to aluminum oxide surface was enhanced by an order of magnitude from nonactivated state to

activated state [28]. When PEG was end-functionalized with nitro-Dopamine, adhesive hydrogels were facilely induced by oxidation or metal coordination, in which light-triggered debonding and degradation were achieved on demand due to the photocleavability of the o-nitrophenyl ethyl moiety [176]. Similarly, a zwitterionic hydrogel was developed with a combination of adhesive catechol functionalities and o-nitrobenzyl crosslinkers. The initial high adhesion strength of 341 kPa could be reduced by 35% upon a short-time (30 min) UV irradiation resulted from the photocleavage of o-nitrobenzyl esters [29]. Locklin and coworkers designed an adhesive hydrogel crosslinked by catechol–Fe^{3+} complexation which was doped with a photo-acid generator [30]. After exposure to UV light, the decrease in pH was induced as a consequence of acid production, resulting in a gel-to-sol transition with a weakened adhesiveness of the material. As pH plays an important role in catechol oxidation, a hydrogel with pH-modulated adhesive/cohesive property was prepared from catechol-conjugated HA [177]. Under acidic conditions, the adhesive polymer could improve the attachment of neural stem cells, while the alkaline-induced hydrogel with strong cohesion was suitable for cell encapsulation. To overcome the limited reversibility provided by oxidation crosslinking, Lee et al. developed a series of hydrogels with completely reversible adhesive/non-adhesive transition based on catechol−boronate complex [108]. As shown in Fig. 8, in an acidic solution (pH 3), both of the catechol and boronic acid moieties contributed to strong interfacial interaction (i.e., hydrogen bonding) with the wetted glass surface, and the work of adhesion measured by contact mechanics test was determined to be 2000 mJ/m^2. At pH 9, the work of adhesion significantly decreased to 180 mJ/m^2, which was ascribed to the formation of the catechol−boronate complex in the network that undermined the interfacial binding. Owing to the reversible nature of this complex and the interfacial interactions, the adhesiveness could be finely and repeatedly tuned by changing pH. With the incorporation of an anionic monomer, acrylic acid,

in the network, a higher pH was required for catechol−boronate complex formation, which preserved the robust interfacial adhesion of the hydrogel in a neutral to mildly basic environment [178]. Huang and coworkers constructed PAPBA-*stat*-PDMA/PGMA/rGO@PDA NC hydrogels by mixing PAPBA-*stat*-PDMA, PGMA, and rGO@PDA in solution. The hydrogels possess excellent pH and glucose responsive sol-gel transitions based on the reversible boronic ester bonds and the strong complexation between glucose and PBA.[179]

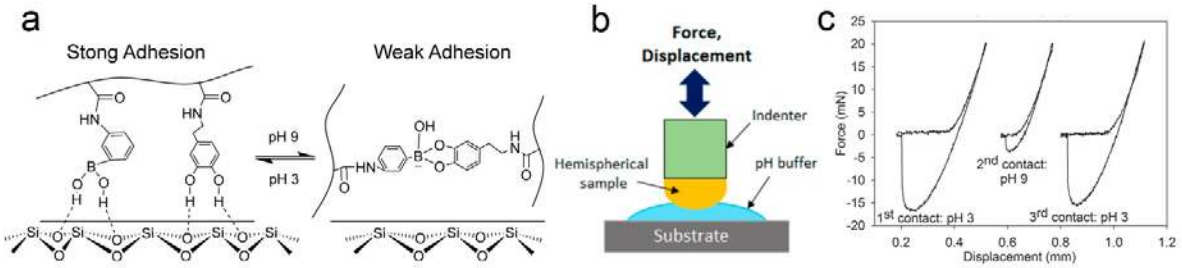

Fig. 8 A smart hydrogel containing catechol and boronic acid functional groups. (a) Schematic illustration of the adhesive/non-adhesive transition of the hydrogel as a function of pH. (b) Schematic representation of the setup for contact mechanics tests. (c) Successive contact curves (pH 3, pH 9, and then pH 3) for the adhesive hydrogel. Reproduced with permission [108]. Copyright © 2016 American Chemical Society

Chao and coworkers designed amyloid protein-based underwater adhesives using recombinant Dopa containing proteins. By pairing LLPS-driven LC domains from humans and Mfp-5 domains, an amyloid forming recombinant protein denoted TDP43 LC-Mfp-5 (TLC-M) experiences phase separation-induced assembly and forms nanofibers, This amyloid protein-based underwater adhesives show strong adhesion energy approaching 48.1 mJ/m^2 and could be applied to "nonstick" surface coating and repairing damage over a wide range of pH and salt conditions[180]. Another functional adhesive nanofibers named (CsgA-Mfp3)-co-(Mfp5-CsgA) are composed of Mfp-3S domains, Mfp-5 domains and CsgA domains generated from an amyloidogenic protein, which also exhibited excellent underwater adhesion energy (~20.9 mJ/m^2) [181]. Furthermore, newly engineered

biofilms have been proposed to take function as cellular glues, with enhanced environmental tolerance and self-regenerating ability [182]. Since Dopa-incorporated recombinant protein adhesives have attracted lots of attention, here we refer readers to several literatures describing the expression of Dopa-incorporated engineered recombinant proteins[183, 184].

3.4 Adhesive polyesters

Synthetic polyesters have been extensively applied in diverse biomedical applications, especially in tissue engineering due to their good mechanical property, easy producibility and controllable biodegradation [185, 186]. Combining adhesive Dopa derivatives with biocompatible polyesters have led to strong tissue adhesives successfully served as bone glues. Wang et al. synthesized a hyperbranched poly(β-amino ester) with Dopamine and triacrylate monomers through Michael addition reaction, which exhibited 37 kPa adhesion strength to wet tissue surface after crosslinking by fibrinogen within 15 min [33]. The low cytotoxic adhesive degraded to 58.5% of the original mass after a month, and the degradation rate could be tailored by optimizing the polymer composition. The mechanical properties of the prepared adhesive were further improved by reinforcement with nano-sized hydroxyapatite particles, and it was demonstrated that the nanocomposite was able to act as efficient bone adhesive for sternal closure with tunable curing speed and sufficient load-bearing capacity [32]. A poly(ester urea)-based adhesive showing adhesive strength comparable with fibrin glue was developed by introducing pendant catechol groups [35], and after the incorporation of poly(propylene glycol) into the backbone, the adhesive was rendered ethanol solubility that is favorable for clinical applications [34]. When a plant-based poly(lactic acid) (PLA) was modified with catechol functionality, the biomimetic adhesive possessed strong adhesion strength of 2.6 MPa in air and 1.0 MPa under wet conditions to aluminum substrates [187]. As indicated in Fig. 9,

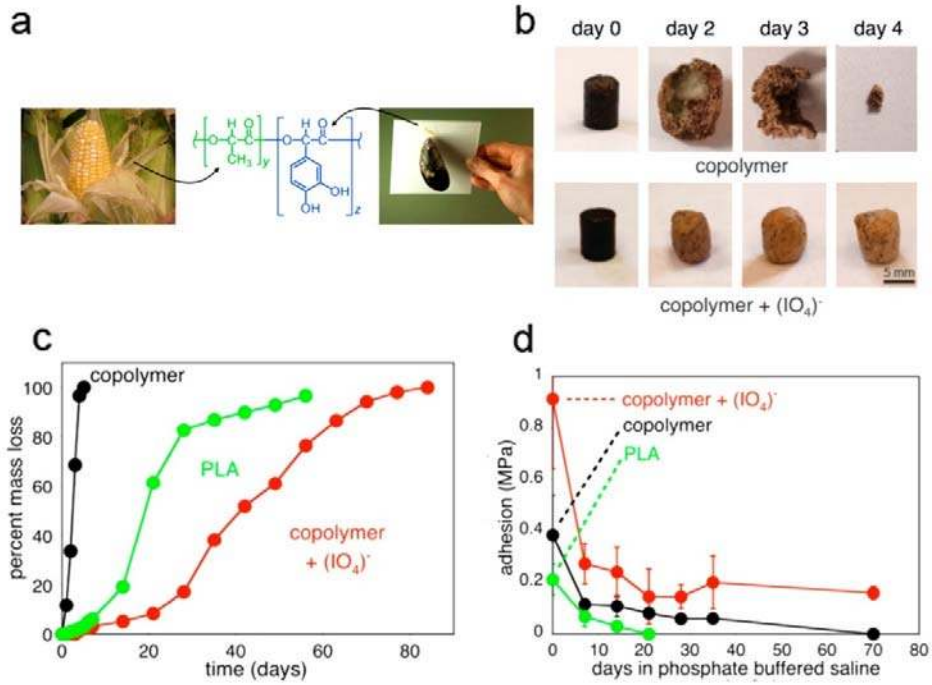

Fig. 9 A catechol-modified PLA adhesive. (a) Schematic representation of the adhesive copolymer combining PLA from corn and mussel-inspired catechol functionality. (b) Degradation of cylindrical samples of catechol-modified PLA with and without periodate crosslinking in phosphate buffered saline (PBS). (c, d) Mass loss and adhesion change of unmodified PLA, catechol-modified PLA (with/without crosslinking) over time when submerged in PBS. Reproduced with permission [187]. Copyright © 2017 American Chemical Society

the hydrolytic degradation of the adhesive could be tailored to be faster or slower than pure PLA by the introduced hydrophilic catechol units and oxidation crosslinking, and the underwater adhesion decreased as a consequence of degradation. Joy et al. reported a polyester adhesive based on catechol-containing soybean oil, where the hydrophobic aliphatic groups facilitated the underwater adhesion (with a lap shear strength of 0.65 MPa to glass surface) by preventing water penetration. Moreover, the low molecular weight of the polyester resulted in a viscous adhesive without requirement of any organic solvents, which is beneficial to surgical applications [188].

Besides the functionalization of catechol groups into the backbone of polyesters, polyDopamine (PDA) deposition on polyester substrates provides a convenient approach to the development of adhesive scaffolds and patches [189]. The PDA coatings on biodegradable poly(ε-caprolactone) (PCL), poly(L-lactide) (PLLA), poly(lactic-co-glycolic acid) (PLGA) and poly(alanine ethyl ester-co-glycine ethyl ester) phosphazene (PAGP) scaffolds were demonstrated to promote the adhesion and proliferation of osteoblast cells, and the enhanced mineralization indicated the potential of this method for bone tissue engineering [40, 190]. By controlling the oxygen supply in the Dopamine solution during deposition, graded PDA coatings were generated on PLLA nanofibers, resulting in a gradient in surface roughness, hydrophilicity and adhesion, and a graded immobilization of various biomolecules including RGD peptide, siRNA and cells was proved [39]. PDA also served as an adhesive layer between a PLLA matrix and bioactive glass nanoparticles, which facilitated the uniform dispersion of nanoparticles and produced a reinforced scaffold [191]. Since PDA not only provides adhesive property but also can bind to metal ions and act as a reducing agent during oxidation, silver conductive patterns on polyester fabric (PET) were fabricated via electroless plating, where Ag nanoparticles were generated by the in situ reduction from Ag^+ with PDA [192]. The silver patterns displayed excellent conductivity (0.86 Ω/sq) and strong adhesion to the flexible fabric, which was ideal for wearable and implantable devices. The readers can refer to some recent reviewer paper on PDA coatings for more details[193-195].

IV CONCLUSIONS AND OUTLOOK

The rapid and robust wet adhesion of marine mussels has been gaining considerable interest in the development of advanced adhesives. The improved understanding of the adhesion mechanisms of

mussel foot proteins reveals that Dopa plays a critical role in the universal adhesion under wet conditions via various interactions including electrostatic interaction, hydrogen bonding, metal-catechol coordination bond, π–π/cation-π interactions, and covalent cross-linking. Combining recombinant Mfps or catecholic moieties with diverse synthetic and natural polymers, a series of mussel-inspired adhesives with on-demand mechanical properties (e.g., viscous coacervates, soft hydrogels and stiff polyesters) and other functionalities have been successfully designed for a broad range of biomedical and engineering applications such as tissue/bone adhesives, drug carriers, surgical implants as well as pollutant adsorbents and plastic adhesives. The pH-responsiveness of catechol-metal coordination and catechol-boronate complexation have been exploited for the preparation of stimuli-responsive materials and smart adhesive. However, catecholic groups generally suffer from oxidation in neutral and basic conditions, which significantly undermines the adhesion and reversibility of the materials and limits their practical applications. Thus, the control of the redox reaction of catechol is necessary for the modulation and optimization of polymer properties.

Multifunctional materials have attracted growing attention nowadays, and adhesive catechol moieties have been combined with polymer networks exhibiting other intriguing properties such as biodegradability, stimuli-responsibility, antibacterial activity and self-healing ability. Since most of the systems are complicated and require tedious synthesis process, it still remains a challenge to develop a facile and universal approach to multifunctional adhesives on demand. Besides the catechol group, other phenolic compounds (e.g., gallic acid, epigallocatechin gallate and tannic acid) also hold promise as building blocks for adhesive materials due to their structural similarity. Compared to catechol-based polymers, these phenol-containing materials are much less reported and are worth further studying due to their easy accessibility and unique properties.

In the mussel plaque, the mussels deliberately control the redox environment of the plaque, which regulates the inner adhesion and cohesion have of the proteins, yet we still lack a complete understanding of how the mussels control the redox environment of the plaque. Moreover, to achieve such redox balance in the catechol-functionalized polymeric adhesive systems is still a tough problem and needs further investigations.

Up to now, the development of mussel-mimetic adhesives has generally focused on the catechol chemistry, but the biological system is far more complex than the Dopa residue. In natural Mfps, other amino acid residues (i.e. cationic, anionic, hydrophobic and thiol groups) also contribute to the strong interfacial binding of mussels to a variety of surfaces by maintaining a balance of different interactions[51, 68, 100, 113]. The synergetic effect between catecholic and cationic moieties in the mussel adhesion system awaits further investigations. Additionally, the mussel plaque also contains various levels of micro and macro structures that are critical to its mechanical properties[126, 196, 197]. More efforts are still needed to incorporate such structures in to the synthetic adhesive systems, which can further promote the design of next-generation adhesives for a broad range of engineering and bioengineering applications.

Acknowledgement

J. Chen and H. Zeng are grateful to the financial support from the Natural Sciences and Engineering Research Council of Canada (NSERC) and the Canada Research Chairs Program. Q. Guo, J. Wang, and J. Yu acknowledge the Singapore National Research Fellowship (NRF-NRFF11-2019-0004) and the AME programmatic funding scheme of Cyber Physiochemical Interfaces (CPI) project #A18A1b0045.

References

1. B. P. Lee, P. B. Messersmith, J. N. Israelachvili and J. H. Waite, *Annu. Rev. Mater. Res.*, 2011, **41**, 99-132.
2. J. Yu, W. Wei, E. Danner, R. K. Ashley, J. N. Israelachvili and J. H. Waite, *Nat. Chem. Biol.*, 2011, **7**, 588.
3. L. Petrone, A. Kumar, C. N. Sutanto, N. J. Patil, S. Kannan, A. Palaniappan, S. Amini, B. Zappone, C. Verma and A. Miserez, *Nat. Commun.*, 2015, **6**, 8737.
4. W. Wei, L. Petrone, Y. Tan, H. Cai, J. N. Israelachvili, A. Miserez and J. H. Waite, *Adv. Funct. Mater.*, 2016, **26**, 3496-3507.
5. E. Bell and J. Gosline, *J. Exp. Biol.*, 1996, **199**, 1005-1017.
6. J. H. Waite, N. H. Andersen, S. Jewhurst and C. Sun, *J. Adhes.*, 2005, **81**, 297-317.
7. E. W. Danner, Y. Kan, M. U. Hammer, J. N. Israelachvili and J. H. Waite, *Biochemistry*, 2012, **51**, 6511-6518.
8. Q. Lu, E. Danner, J. H. Waite, J. N. Israelachvili, H. Zeng and D. S. Hwang, *J. R. Soc., Interface*, 2013, **10**.
9. J. Yu, W. Wei, M. S. Menyo, A. Masic, J. H. Waite and J. N. Israelachvili, *Biomacromolecules*, 2013, **14**, 1072-1077.
10. J. Yu, Y. Kan, M. Rapp, E. Danner, W. Wei, S. Das, D. R. Miller, Y. Chen, J. H. Waite and J. N. Israelachvili, *Proc. Natl. Acad. Sci.*, 2013, **110**, 15680-15685.
11. S. H. Donaldson, S. Das, M. A. Gebbie, M. Rapp, L. C. Jones, Y. Roiter, P. H. Koenig, Y. Gizaw and J. N. Israelachvili, *ACS Nano*, 2013, **7**, 10094-10104.
12. H. J. Kim, B.-H. Choi, S. H. Jun and H. J. Cha, *Adv. Healthcare Mater.*, 2016, **5**, 3191-3202.
13. H. J. Kim, B. H. Hwang, S. Lim, B.-H. Choi, S. H. Kang and H. J. Cha, *Biomaterials*, 2015, **72**, 104-111.
14. D. S. Hwang, H. Zeng, A. Srivastava, D. V. Krogstad, M. Tirrell, J. N. Israelachvili and J. H. Waite, *Soft Matter*, 2010, **6**, 3232-3236.
15. S. Lim, Y. S. Choi, D. G. Kang, Y. H. Song and H. J. Cha, *Biomaterials*, 2010, **31**, 3715-3722.
16. D. W. R. Balkenende, S. M. Winkler and P. B. Messersmith, *Eur. Polym. J.*, 2019, **116**, 134-143.
17. A. H. Hofman, I. A. van Hees, J. Yang and M. Kamperman, *Adv. Mater.*, 2018, **30**, 1704640.
18. V. Bhagat and M. L. Becker, *Biomacromolecules*, 2017, **18**, 3009-3039.
19. L. Li and H. Zeng, *Biotribology*, 2016, **5**, 44-51.
20. L. Li, W. Smitthipong and H. Zeng, *Polym. Chem.*, 2015, **6**, 353-358.
21. J. H. Waite, *J. Exp. Biol.*, 2017, **220**, 517.
22. S. Kim, J. Huang, Y. Lee, S. Dutta, H. Y. Yoo, Y. M. Jung, Y. Jho, H. Zeng and D. S. Hwang, *Proc. Natl. Acad. Sci.*, 2016, **113**, E847-853.
23. D. R. Miller, S. Das, K. Y. Huang, S. Han, J. N. Israelachvili and J. H. Waite, *ACS Biomater. Sci. Eng.*, 2015, **1**, 1121-1128.
24. C. E. Brubaker and P. B. Messersmith, *Biomacromolecules*, 2011, **12**, 4326-4334.

25. T. Chen, Y. Chen, H. U. Rehman, Z. Chen, Z. Yang, M. Wang, H. Li and H. Liu, *ACS Appl. Mater. Interfaces*, 2018, **10**, 33523–33531.
26. L. Han, L. Yan, M. Wang, K. Wang, L. Fang, J. Zhou, J. Fang, F. Ren and X. Lu, *Chem. Mater.*, 2018, **30**, 5561-5572.
27. M. Krogsgaard, M. A. Behrens, J. S. Pedersen and H. Birkedal, *Biomacromolecules*, 2013, **14**, 297-301.
28. P. Wilke, N. Helfricht, A. Mark, G. Papastavrou, D. Faivre and H. G. Borner, *J. Am. Chem. Soc.*, 2014, **136**, 12667-12674.
29. M. Kim and H. Chung, *Polym. Chem.*, 2017, **8**, 6300-6308.
30. E. M. White, J. E. Seppala, P. M. Rushworth, B. W. Ritchie, S. Sharma and J. Locklin, *Macromolecules*, 2013, **46**, 8882-8887.
31. P. Wilke and H. G. Börner, *ACS Macro Lett.*, 2012, **1**, 871-875.
32. H. Zhang, L. Bré, T. Zhao, B. Newland, M. Da Costa and W. Wang, *J. Mater. Chem. B*, 2014, **2**, 4067-4071.
33. H. Zhang, L. P. Bré, T. Zhao, Y. Zheng, B. Newland and W. Wang, *Biomaterials*, 2014, **35**, 711-719.
34. J. Zhou, V. Bhagat and M. L. Becker, *ACS Appl. Mater. Interfaces*, 2016, **8**, 33423-33429.
35. J. Zhou, A. P. Defante, F. Lin, Y. Xu, J. Yu, Y. Gao, E. Childers, A. Dhinojwala and M. L. Becker, *Biomacromolecules*, 2015, **16**, 266-274.
36. A. Kawamura, A. Harada, K. Kono and K. Kataoka, *Bioconjugate Chem.*, 2007, **18**, 1555-1559.
37. A. Harada and K. Kataoka, *J. Controlled Release*, 2001, **72**, 85-91.
38. L. Schoonen and J. C. M. van Hest, *Adv. Mater.*, 2016, **28**, 1109-1128.
39. S. K. M. Perikamana, Y. M. Shin, J. K. Lee, Y. B. Lee, Y. Heo, T. Ahmad, S. Y. Park, J. Shin, K. M. Park and H. S. Jung, *Colloids Surf. B. Biointerfaces*, 2017, **159**, 546-556.
40. W. B. Tsai, W. T. Chen, H. W. Chien, W. H. Kuo and M. J. Wang, *J. Biomater. Appl.*, 2014, **28**, 837-848.
41. Q. Wang and J. B. Schlenoff, *Macromolecules*, 2014, **47**, 3108-3116.
42. E. A. Frankel, P. C. Bevilacqua and C. D. Keating, *Langmuir*, 2016, **32**, 2041-2049.
43. N. Pippa, M. Karayianni, S. Pispas and C. Demetzos, *Int. J. Pharm.*, 2015, **491**, 136-143.
44. N. R. Martinez Rodriguez, S. Das, Y. Kaufman, J. N. Israelachvili and J. H. Waite, *Biofouling*, 2015, **31**, 221-227.
45. J. H. Waite, *J. Exp. Biol.*, 2017, **220**, 517-530.
46. J. H. Waite, T. J. Housley and M. L. Tanzer, *Biochemistry*, 1985, **24**, 5010-5014.
47. D. S. Hwang and J. H. Waite, *Protein Sci.*, 2012, **21**, 1689-1695.
48. K. Inoue, Y. Takeuchi, D. Miki and S. Odo, *J. Biol. Chem.*, 1995, **270**, 6698-6701.
49. R. Mirshafian, W. Wei, J. N. Israelachvili and J. H. Waite, *Biochemistry*, 2016, **55**, 743-750.
50. V. V. Papov, T. V. Diamond, K. Biemann and J. H. Waite, *J. Biol. Chem.*, 1995, **270**, 20183-20192.
51. W. Wei, Y. Tan, N. R. Martinez Rodriguez, J. Yu, J. N. Israelachvili and J. H. Waite, *Acta Biomater.*, 2014, **10**, 1663-1670.
52. S. Seo, S. Das, P. J. Zalicki, R. Mirshafian, C. D. Eisenbach, J. N. Israelachvili, J. H. Waite and B. K. Ahn, *J. Am. Chem. Soc.*, 2015, **137**, 9214-9217.
53. H. Zhao and J. H. Waite, *Biochemistry*, 2006, **45**, 14223-14231.
54. J. H. Waite and X. Qin, *Biochemistry*, 2001, **40**, 2887-2893.
55. H. Lee, S. M. Dellatore, W. M. Miller and P. B. Messersmith, *Science*, 2007, **318**, 426-430.
56. H. Zhao and J. H. Waite, *J. Biol. Chem.*, 2006, **281**, 26150-26158.
57. X.-X. Qin, K. J. Coyne and J. H. Waite, *J. Biol. Chem.*, 1997, **272**, 32623-32627.
58. A. A. Arnold, F. Byette, M.-O. Séguin-Heine, A. LeBlanc, L. Sleno, R. Tremblay, C. Pellerin and I. Marcotte, *Biomacromolecules*, 2013, **14**, 132-141.

59. J. Sagert and J. H. Waite, *J. Exp. Biol.*, 2009, **212**, 2224-2236.
60. K. J. Coyne, X.-X. Qin and J. H. Waite, *Science*, 1997, **277**, 1830-1832.
61. J. H. Waite, X.-X. Qin and K. J. Coyne, *Matrix Biol.*, 1998, **17**, 93-106.
62. C. Sun, J. M. Lucas and J. H. Waite, *Biomacromolecules*, 2002, **3**, 1240-1248.
63. M. H. Suhre, M. Gertz, C. Steegborn and T. Scheibel, *Nat. Commun.*, 2014, **5**, 3392.
64. M. P. Deacon, S. S. Davis, J. H. Waite and S. E. Harding, *Biochemistry*, 1998, **37**, 14108-14112.
65. L. M. Rzepecki, K. M. Hansen and J. H. Waite, *Biol. Bull.*, 1992, **183**, 123-137.
66. Y. Kan, E. W. Danner, J. N. Israelachvili, Y. Chen and J. H. Waite, *PLOS ONE*, 2014, **9**, e108869.
67. T. Priemel, E. Degtyar, M. N. Dean and M. J. Harrington, *Nat. Commun.*, 2017, **8**, 14539.
68. J. Yu, W. Wei, E. Danner, R. K. Ashley, J. N. Israelachvili and J. H. Waite, *Nat. Chem. Biol.*, 2011, **7**, 588-590.
69. L. Petrone, A. Kumar, C. N. Sutanto, N. J. Patil, S. Kannan, A. Palaniappan, S. Amini, B. Zappone, C. Verma and A. Miserez, *Nat. Commun.*, 2015, **6**, 8737.
70. D. Miki, Y. Takeuchi, K. Inoue and S. Odo, *Biol. Bull.*, 1996, **190**, 213-217.
71. I. Kaminker, W. Wei, A. M. Schrader, Y. Talmon, M. T. Valentine, J. N. Israelachvili, J. H. Waite and S. Han, *Soft Matter*, 2017, **13**, 9122-9131.
72. J. Yu, in *Adhesive Interactions of Mussel Foot Proteins*, ed. J. Yu, Springer International Publishing, Cham, 2014, DOI: 10.1007/978-3-319-06031-6_4, pp. 31-41.
73. M. H. Suhre, M. Gertz, C. Steegborn and T. Scheibel, *Nat. Commun.*, 2014, **5**, 3392.
74. H. Y. Yoo, J. Huang, L. Li, M. Foo, H. Zeng and D. S. Hwang, *Biomacromolecules*, 2016, **17**, 946-953.
75. J. Wang, M. N. Tahir, M. Kappl, W. Tremel, N. Metz, M. Barz, P. Theato and H.-J. Butt, *Adv. Mater.*, 2008, **20**, 3872-3876.
76. Y. Li, C. Liang, L. Gao, S. Li, Y. Zhang, J. Zhang and Y. Cao, *Mater. Chem. Front.*, 2017, **1**, 2664-2668.
77. J. L. Dalsin, B.-H. Hu, B. P. Lee and P. B. Messersmith, *J. Am. Chem. Soc.*, 2003, **125**, 4253-4258.
78. J. Kuang and P. B. Messersmith, *Langmuir*, 2012, **28**, 7258-7266.
79. Y. Lee, H. Lee, Y. B. Kim, J. Kim, T. Hyeon, H. Park, P. B. Messersmith and T. G. Park, *Adv. Mater.*, 2008, **20**, 4154-4157.
80. B. Julien, M. Angela, D. Camille, G. Guillaume, L. Philippe, H. Vincent Le, M. Garrett Brian and V. Nihal Engin, *Biomed. Mater.*, 2018, **13**, 015015.
81. N. Holten-Andersen, M. J. Harrington, H. Birkedal, B. P. Lee, P. B. Messersmith, K. Y. C. Lee and J. H. Waite, *Proc. Natl. Acad. Sci.*, 2011, **108**, 2651-2655.
82. Q. Ye, F. Zhou and W. Liu, *Chem. Soc. Rev.*, 2011, **40**, 4244-4258.
83. Z. Xu, *Sci. Rep.*, 2013, **3**, 2914-2914.
84. M. J. Sever, J. T. Weisser, J. Monahan, S. Srinivasan and J. J. Wilker, *Angew. Chem. Int. Ed.*, 2004, **43**, 448-450.
85. Q. Lu, D. X. Oh, Y. Lee, Y. Jho, D. S. Hwang and H. Zeng, *Angew. Chem. Int. Ed.*, 2013, **52**, 3944-3948.
86. D. S. Hwang, H. Zeng, Q. Lu, J. Israelachvili and J. H. Waite, *Soft Matter*, 2012, **8**, 5640-5648.
87. S. Kim, A. Faghihnejad, Y. Lee, Y. Jho, H. Zeng and D. S. Hwang, *J. Mater. Chem. B*, 2015, **3**, 738-743.
88. S. C. T. Nicklisch and J. H. Waite, *Biofouling*, 2012, **28**, 865-877.
89. J. J. Wilker, *Angew. Chem. Int. Ed.*, 2010, **49**, 8076-8078.
90. J. Yu, W. Wei, E. Danner, J. N. Israelachvili and J. H. Waite, *Adv. Mater.*, 2011, **23**, 2362-2366.
91. B. Yang, C. Lim, D. S. Hwang and H. J. Cha, *Chem. Mater.*, 2016, **28**, 7982-7989.
92. N. R. Martinez Rodriguez, S. Das, Y. Kaufman, W. Wei, J. N. Israelachvili and J. H. Waite, *Biomaterials*, 2015, **51**, 51-57.
93. B. K. Ahn, D. W. Lee, J. N. Israelachvili and J. H. Waite, *Nat. Mater.*, 2014, **13**, 867.

94. H. Zeng, D. S. Hwang, J. N. Israelachvili and J. H. Waite, *Proc. Natl. Acad. Sci.*, 2010, **107**, 12850-12853.
95. M. J. Harrington, A. Masic, N. Holten-Andersen, J. H. Waite and P. Fratzl, *Science*, 2010, **328**, 216.
96. J. H. Waiter, *Ann. N.Y. Acad. Sci.*, 1999, **875**, 301-309.
97. W. Wei, J. Yu, M. A. Gebbie, Y. Tan, N. R. Martinez Rodriguez, J. N. Israelachvili and J. H. Waite, *Langmuir*, 2015, **31**, 1105-1112.
98. M. A. Gebbie, W. Wei, A. M. Schrader, T. R. Cristiani, H. A. Dobbs, M. Idso, B. F. Chmelka, J. H. Waite and J. N. Israelachvili, *Nat. Chem.*, 2017, **9**, 723-723.
99. M. V. Rapp, G. P. Maier, H. A. Dobbs, N. J. Higdon, J. H. Waite, A. Butler and J. N. Israelachvili, *J. Am. Chem. Soc.*, 2016, **138**, 9013-9016.
100. G. P. Maier, M. V. Rapp, J. H. Waite, J. N. Israelachvili and A. Butler, *Science*, 2015, **349**, 628.
101. T. J. Deming, *Curr. Opin. Chem. Biol.*, 1999, **3**, 100-105.
102. H. G. Silverman and F. F. Roberto, *Mar. Biotechnol.*, 2007, **9**, 661-681.
103. S.-C. Li, L.-N. Chu, X.-Q. Gong and U. Diebold, *Science*, 2010, **328**, 882.
104. S. Bahri, C. M. Jonsson, C. L. Jonsson, D. Azzolini, D. A. Sverjensky and R. M. Hazen, *Environ. Sci. Technol.*, 2011, **45**, 3959-3966.
105. S. A. Mian, L.-M. Yang, L. C. Saha, E. Ahmed, M. Ajmal and E. Ganz, *Langmuir*, 2014, **30**, 6906-6914.
106. H. Lee, N. F. Scherer and P. B. Messersmith, *Proc. Natl. Acad. Sci.*, 2006, **103**, 12999-13003.
107. L. Schmitt, M. Ludwig, H. E. Gaub and R. Tampé, *Biophys. J.*, 2000, **78**, 3275-3285.
108. A. R. Narkar, B. Barker, M. Clisch, J. Jiang and B. P. Lee, *Chem. Mater.*, 2016, **28**, 5432-5439.
109. S.-C. Li, L.-N. Chu, X.-Q. Gong and U. Diebold, *Science*, 2010, **328**, 882-884.
110. K. Kendall, *Science*, 1994, **263**, 1720-1725.
111. T. H. Anderson, J. Yu, A. Estrada, M. U. Hammer, J. H. Waite and J. N. Israelachvili, *Adv. Funct. Mater.*, 2010, **20**, 4196-4205.
112. T. Fukuma, Y. Ueda, S. Yoshioka and H. Asakawa, *Phys. Rev. Lett.*, 2010, **104**, 016101.
113. Q. Lin, D. Gourdon, C. Sun, N. Holten-Andersen, T. H. Anderson, J. H. Waite and J. N. Israelachvili, *Proc. Natl. Acad. Sci.*, 2007, **104**, 3782.
114. Q. Lu, D. S. Hwang, Y. Liu and H. Zeng, *Biomaterials*, 2012, **33**, 1903-1911.
115. L. M. Salonen, M. Ellermann and F. Diederich, *Angew. Chem. Int. Ed.*, 2011, **50**, 4808-4842.
116. C. G. De Kruif, F. Weinbreck and R. de Vries, *Curr. Opin. Colloid Interface Sci.*, 2004, **9**, 340-349.
117. H. Shao and R. J. Stewart, *Adv. Mater.*, 2010, **22**, 729-733.
118. M. Renner-Rao, M. Clark and M. J. Harrington, *Langmuir*, 2019, **35**, 15992-16001.
119. A. P. Imeson, D. A. Ledward and J. R. Mitchell, *J. Sci. Food Agric.*, 1977, **28**, 661-668.
120. D. Priftis, L. Leon, Z. Song, S. L. Perry, K. O. Margossian, A. Tropnikova, J. Cheng and M. Tirrell, *Angew. Chem.*, 2015, **127**, 11280-11284.
121. K. A. Black, D. Priftis, S. L. Perry, J. Yip, W. Y. Byun and M. Tirrell, *ACS Macro Lett.*, 2014, **3**, 1088-1091.
122. E. Kizilay, A. B. Kayitmazer and P. L. Dubin, *Adv. Colloid Interface Sci.*, 2011, **167**, 24-37.
123. J. van der Gucht, E. Spruijt, M. Lemmers and M. A. Cohen Stuart, *J. Colloid Interface Sci.*, 2011, **361**, 407-422.
124. B. de Jong, 1929.
125. H. Shao, K. N. Bachus and R. J. Stewart, *Macromol. Biosci.*, 2009, **9**, 464-471.
126. Q. Zhao, D. W. Lee, B. K. Ahn, S. Seo, Y. Kaufman, J. N. Israelachvili and J. H. Waite, *Nat. Mater.*, 2016, **15**, 407-412.
127. J. Wang and T. Scheibel, *Biomacromolecules*, 2018, **19**, 3612-3619.
128. W. Wei, Y. Tan, N. R. Martinez Rodriguez, J. Yu, J. N. Israelachvili and J. H. Waite, *Acta Biomater*, 2014, **10**, 1663-1670.

129. W. Wei, J. Yu, C. Broomell, J. N. Israelachvili and J. H. Waite, *J. Am. Chem. Soc.*, 2013, **135**, 377-383.
130. B. K. Ahn, S. Das, R. Linstadt, Y. Kaufman, N. R. Martinez-Rodriguez, R. Mirshafian, E. Kesselman, Y. Talmon, B. H. Lipshutz, J. N. Israelachvili and J. H. Waite, *Nat. Commun.*, 2015, **6**, 8663.
131. S. Kim, H. Y. Yoo, J. Huang, Y. Lee, S. Park, Y. Park, S. Jin, Y. M. Jung, H. Zeng and D. S. Hwang, *ACS nano*, 2017, **11**, 6764-6772.
132. A. S. Hoffman, *Adv. Drug Del. Rev.*, 2012, **64**, 18-23.
133. E. Caló and V. V. Khutoryanskiy, *Eur. Polym. J.*, 2015, **65**, 252-267.
134. N. Annabi, A. Tamayol, S. R. Shin, A. M. Ghaemmaghami, N. A. Peppas and A. Khademhosseini, *Nano Today*, 2014, **9**, 574-589.
135. B. P. Lee, J. L. Dalsin and P. B. Messersmith, *Biomacromolecules*, 2002, **3**, 1038-1047.
136. B. P. Lee, K. Huang, F. N. Nunalee, K. R. Shull and P. B. Messersmith, *J. Biomater. Sci., Polym. Ed.*, 2004, **15**, 449-464.
137. B. P. Lee, C.-Y. Chao, F. N. Nunalee, E. Motan, K. R. Shull and P. B. Messersmith, *Macromolecules*, 2006, **39**, 1740-1748.
138. C. E. Brubaker, H. Kissler, L. J. Wang, D. B. Kaufman and P. B. Messersmith, *Biomaterials*, 2010, **31**, 420-427.
139. M. Mehdizadeh, H. Weng, D. Gyawali, L. Tang and J. Yang, *Biomaterials*, 2012, **33**, 7972-7983.
140. D. Xie, J. Guo, M. Mehdizadeh, R. T. Tran, R. Chen, D. Sun, G. Qian, D. Jin, X. Bai and J. Yang, *J. Mater. Chem. B*, 2015, **3**, 387-398.
141. H. Zhang, T. Zhao, B. Newland, P. Duffy, A. N. Annaidh, E. D. O'Cearbhaill and W. Wang, *J. Mater. Chem. B*, 2015, **3**, 6420-6428.
142. Z. Liu, Y. Jiao, Y. Wang, C. Zhou and Z. Zhang, *Adv. Drug Del. Rev.*, 2008, **60**, 1650-1662.
143. Y. Lee, H. J. Chung, S. Yeo, C.-H. Ahn, H. Lee, P. B. Messersmith and T. G. Park, *Soft Matter*, 2010, **6**, 977-983.
144. J. H. Ryu, Y. Lee, W. H. Kong, T. G. Kim, T. G. Park and H. Lee, *Biomacromolecules*, 2011, **12**, 2653-2659.
145. C. Lee, J. Shin, J. S. Lee, E. Byun, J. H. Ryu, S. H. Um, D. I. Kim, H. Lee and S. W. Cho, *Biomacromolecules*, 2013, **14**, 2004-2013.
146. J. Shin, J. S. Lee, C. Lee, H. J. Park, K. Yang, Y. Jin, J. H. Ryu, K. S. Hong, S. H. Moon and H. M. Chung, *Adv. Funct. Mater.*, 2015, **25**, 3814-3824.
147. Y. C. Choi, J. S. Choi, Y. J. Jung and Y. W. Cho, *J. Mater. Chem. B*, 2014, **2**, 201-209.
148. W. Chen, R. Wang, T. Xu, X. Ma, Z. Yao, B. Chi and H. Xu, *J. Mater. Chem. B*, 2017, **5**, 5668-5678.
149. R. Wang, J. Li, W. Chen, T. Xu, S. Yun, Z. Xu, Z. Xu, T. Sato, B. Chi and H. Xu, *Adv. Funct. Mater.*, 2017, **27**, 1604894.
150. S. Yan, W. Wang, X. Li, J. Ren, W. Yun, K. Zhang, G. Li and J. Yin, *J. Mater. Chem. B*, 2018, **6**, 6377-6390.
151. B. J. Kim, D. X. Oh, S. Kim, J. H. Seo, D. S. Hwang, A. Masic, D. K. Han and H. J. Cha, *Biomacromolecules*, 2014, **15**, 1579-1585.
152. L. Yu and J. Ding, *Chem. Soc. Rev.*, 2008, **37**, 1473-1481.
153. P. Zhao, K. Wei, Q. Feng, H. Chen, D. S. H. Wong, X. Chen, C. C. Wu and L. Bian, *Chem. Commun. (Cambridge, U. K.)*, 2017, **53**, 12000-12003.
154. N. Pandey, A. Hakamivala, C. Xu, P. Hariharan, B. Radionov, Z. Huang, J. Liao, L. Tang, P. Zimmern and K. T. Nguyen, *Adv. Healthcare Mater.*, 2018, **7**, 1701069.
155. L. Han, X. Lu, K. Liu, K. Wang, L. Fang, L. T. Weng, H. Zhang, Y. Tang, F. Ren, C. Zhao, G. Sun, R. Liang and Z. Li, *ACS Nano*, 2017, **11**, 2561-2574.

156. L. Han, X. Lu, M. Wang, D. Gan, W. Deng, K. Wang, L. Fang, K. Liu, C. W. Chan and Y. Tang, *Small*, 2017, **13**, 1601916.
157. A. Cholewinski, F. Yang and B. Zhao, *Mater. Horiz.*, 2019, **6**, 285-293.
158. L. Han, K. Liu, M. Wang, K. Wang, L. Fang, H. Chen, J. Zhou and X. Lu, *Adv. Funct. Mater.*, 2018, **28**, 1704195.
159. I. Erel-Unal and S. A. Sukhishvili, *Macromolecules*, 2008, **41**, 3962-3970.
160. K. Kim, M. Shin, M. Y. Koh, J. H. Ryu, M. S. Lee, S. Hong and H. Lee, *Adv. Funct. Mater.*, 2015, **25**, 2402-2410.
161. H. Fan, J. Wang, Q. Zhang and Z. Jin, *ACS Omega*, 2017, **2**, 6668-6676.
162. H. Fan, J. Wang and Z. Jin, *Macromolecules*, 2018, **51**, 1696-1705.
163. C. Shao, M. Wang, L. Meng, H. Chang, B. Wang, F. Xu, J. Yang and P. Wan, *Chem. Mater.*, 2018, **30**, 3110-3121.
164. N. Holten-Andersen, A. Jaishankar, M. J. Harrington, D. E. Fullenkamp, G. DiMarco, L. He, G. H. McKinley, P. B. Messersmith and K. Y. C. Lee, *J. Mater. Chem. B*, 2014, **2**, 2467-2472.
165. M. Krogsgaard, M. R. Hansen and H. Birkedal, *J. Mater. Chem. B*, 2014, **2**, 8292-8297.
166. A. Andersen, M. Krogsgaard and H. Birkedal, *Biomacromolecules*, 2018, **19**, 1402-1409.
167. N. Chen, L. Qin and Q. Pan, *J. Mater. Chem. A*, 2018, **6**, 6667-6674.
168. M. Nakahata, S. Mori, Y. Takashima, A. Hashidzume, H. Yamaguchi and A. Harada, *ACS Macro Lett.*, 2014, **3**, 337-340.
169. M. Shan, C. Gong, B. Li and G. Wu, *Polym. Chem.*, 2017, **8**, 2997-3005.
170. Y. Chen, D. Diaz-Dussan, D. Wu, W. Wang, Y.-Y. Peng, A. B. Asha, D. G. Hall, K. Ishihara and R. Narain, *ACS Macro Lett.*, 2018, **7**, 904-908.
171. L. Li, B. Yan, J. Yang, L. Chen and H. Zeng, *Adv. Mater.*, 2015, **27**, 1294-1299.
172. L. Li, B. Yan, J. Yang, W. Huang, L. Chen and H. Zeng, *ACS Appl. Mater. Interfaces*, 2017, **9**, 9221-9225.
173. R. Bogue, *Assembly Autom.*, 2011, **31**, 207-211.
174. C. Heinzmann, S. Coulibaly, A. Roulin, G. L. Fiore and C. Weder, *ACS Appl. Mater. Interfaces*, 2014, **6**, 4713-4719.
175. M. T. Northen, C. Greiner, E. Arzt and K. L. Turner, *Adv. Mater.*, 2008, **20**, 3905-3909.
176. Z. Shafiq, J. Cui, L. Pastor-Perez, V. San Miguel, R. A. Gropeanu, C. Serrano and A. del Campo, *Angew. Chem. Int. Ed. Engl.*, 2012, **51**, 4332-4335.
177. S. Hong, K. Yang, B. Kang, C. Lee, I. T. Song, E. Byun, K. I. Park, S. W. Cho and H. Lee, *Adv. Funct. Mater.*, 2013, **23**, 1774-1780.
178. A. R. Narkar and B. P. Lee, *Langmuir*, 2018, **34**, 9410-9417.
179. W. Huang, C. Qi and Y. Gao, *ACS Appl. Nano Mater.*, 2019, **2**, 5000-5008.
180. M. Cui, X. Wang, B. An, C. Zhang, X. Gui, K. Li, Y. Li, P. Ge, J. Zhang, C. Liu and C. Zhong, *Sci. Adv.*, 2019, **5**, eaax3155.
181. C. Zhong, T. Gurry, A. A. Cheng, J. Downey, Z. Deng, C. M. Stultz and T. K. Lu, *Nat. Nanotechnol.*, 2014, **9**, 858-866.
182. C. Zhang, J. Huang, J. Zhang, S. Liu, M. Cui, B. An, X. Wang, J. Pu, T. Zhao, C. Fan, T. K. Lu and C. Zhong, *Mater. Today*, 2019, **28**, 40-48.
183. M. Hauf, F. Richter, T. Schneider, T. Faidt, B. M. Martins, T. Baumann, P. Durkin, H. Dobbek, K. Jacobs, A. Möglich and N. Budisa, *ChemBioChem*, 2017, **18**, 1819-1823.
184. B. Yang, N. Ayyadurai, H. Yun, Y. S. Choi, B. H. Hwang, J. Huang, Q. Lu, H. Zeng and H. J. Cha, *Angew. Chem. Int. Ed.*, 2014, **53**, 13360-13364.
185. R. P. Brannigan and A. P. Dove, *Biomater. Sci.*, 2017, **5**, 9-21.
186. S. A. Park, S. H. Lee and W. D. Kim, *Bioprocess Biosystems Eng.*, 2011, **34**, 505-513.

187. C. L. Jenkins, H. M. Siebert and J. J. Wilker, *Macromolecules*, 2017, **50**, 561-568.
188. Y. Xu, Q. Liu, A. Narayanan, D. Jain, A. Dhinojwala and A. Joy, *Adv. Mater. Interfaces*, 2017, **4**, 1700506.
189. S. K. M. Perikamana, J. Lee, Y. B. Lee, Y. M. Shin, E. J. Lee, A. G. Mikos and H. Shin, *Biomacromolecules*, 2015, **16**, 2541-2555.
190. Y. Li, Y. Shi, S. Duan, D. Shan, Z. Wu, Q. Cai and X. Yang, *J. Biomed. Mater. Res.*, 2014, **102**, 3894-3902.
191. Y. Xu, P. Wu, P. Feng, W. Guo, W. Yang and C. Shuai, *Colloids Surf. B. Biointerfaces*, 2018, **170**, 45-53.
192. Y. Mao, M. Zhu, W. Wang and D. Yu, *Soft Matter*, 2018, **14**, 1260-1269.
193. M. E. Lynge, R. van der Westen, A. Postma and B. Städler, *Nanoscale*, 2011, **3**, 4916-4928.
194. J. H. Ryu, P. B. Messersmith and H. Lee, *ACS Appl. Mater. Interfaces*, 2018, **10**, 7523-7540.
195. Y. H. Ding, M. Floren and W. Tan, *Biosurf. Biotribol.*, 2016, **2**, 121-136.
196. D. G. Barrett, D. E. Fullenkamp, L. He, N. Holten-Andersen, K. Y. C. Lee and P. B. Messersmith, *Adv. Funct. Mater.*, 2013, **23**, 1111-1119.
197. M. S. Menyo, C. J. Hawker and J. H. Waite, *ACS Macro Lett.*, 2015, **4**, 1200-1204.